Journal of Nanofluids
Vol. 12, pp. 1298–1319, 2023
(www.aspbs.com/jon)

ARTICLE

Magnetohydrodynamic (MHD) Natural Convection Flow of Titanium Dioxide Nanofluid Inside 3D Cavity Containing a Hot Block: Comparative with 2D Cavity

Mourad Moderres[1,*], Abdelkader Boutra[2], Seddik Kherroubi[2], Hakan F. Oztop[3], and Youb Khaled Benkahla[2]

[1]*Laboratory of Industrial Fluids, Measurements and Application (FIMA) UDBKM, Ain Defla, 44225, Algeria*
[2]*Laboratory of Transport Phenomena, USTHB, BP. 32 El Alia, Bab Ezzouar, Algiers, 16111, Algeria*
[3]*Department of Mechanical Engineering, Technology Faculty, Fırat University, Elazığ, 23119, Turkey*

The natural convection of TiO_2-Water-Nanofluid in a cubic cavity, containing a hot block under the influence of the magnetic field was studied numerically. The verticals walls are cold, the bottom wall is hot and the other walls (top, front and rear) are adiabatic. This work aims to visualize the importance of taking into account the three-dimensionality of the flow in the presence of magnetic field as well as the impact of the addition of nanoparticles on heat exchange rate evolution. The governing equations are solved using the finite volume method and the SIMPLER algorithm is used for pressure-velocity coupling. The problem was simulated at different Rayleigh numbers ($10^3 \leq Ra \leq 10^6$), Hartmann numbers ($0 \leq Ha \leq 90$) and inclination angles of the magnetic field ($0 \leq \omega \leq 135°$) as well as nanoparticles volume fraction ($\varphi = 0\%$, $\varphi = 5\%$) with fixed Prandtl number ($Pr = 7$). The thermal conductivity and dynamic viscosity of the nanofluid are estimated by taking into account temperature-dependent properties, using Corcione's correlations. Based on the cooling optimization of cold walls along with comparative analysis between 3D cavity and 2D cavity, the obtained results show that the buoyancy force enhances the heat exchange, while the magnetic field produces opposite effects. When the buoyancy force is dominated, the intensification of heat transfer becomes large, compared to the case where conduction is dominant. The qualitative difference between a 3D and 2D configuration is remarkable for higher Ra, and becomes smaller when the magnetic field is applied horizontally or vertically with relatively high intensity. But, quantitatively, the 3D flow is far from being considered as a 2D flow for all pertinent parameters control. Finally, adding nanoparticles enhances heat transfer for both configurations, the best transfer rate is obtained for $\omega = 0$.

KEYWORDS: Magnetoconvection, Nanofluid, 3D and 2D Configurations, Hartmann Number, Thermal Conductivity.

1. INTRODUCTION

Magnetoconvection flow in the enclosures is one of the most studied problems in thermal engineering when fluid movement is caused by buoyancy forces due to the density difference between two regions (i.e., natural convection), and under the Lorentz forces effect, due to the applied magnetic field (i.e., natural convection under the presence of magnetic field; Magnetoconvection). This flow is encountered in various heat exchange processes applications, including the cooling of electronic devices, lubrication technologies, solar power collectors, drying technologies, chemical processing equipment, and others.[1–5]

During the last few decades, to enhance the convective heat transfer, one of the promising solutions is to modify the working fluids characteristics, by increasing their thermal conductivities, consequently resulting in significant enhancements in the heat transfer coefficients. Nanofluids, which are a new class of fluids obtained by dispersing nanoparticles in base fluids, have been considered as a promising alternative heat transfer fluid and were first reported by Choi and Eastman.[6] Currently, these fluids (nanofluids) are widely used in cooling systems for solar collectors, boiling reactor systems, as well as to improve vehicle cooling systems.[7–9] In the work of Vanaki et al.,[10] we clearly see that the injection of nanoparticles in heat transfer fluids improves the rate of heat exchange, where the estimation of improvement rate depends on

*Author to whom correspondence should be addressed.
Email: mouradw002@gmail.com
Received: 7 July 2022
Accepted: 16 October 2022

several factors, such as type of nanoparticle, nanoparticle volume concentration, nanoparticle shape size and shape of nanoparticles, and particle movement. In addition, a synthesis of research on the metal oxide nanofluids, thermophysical properties, preparation, mechanisms at the molecular status influencing transport properties and examination of nanofluids for cooling systems. The influences of nanofluid formulation and material parameters such as nanomaterial morphology, temperature, additives, and the viscosity of base fluid on the transport properties of nanofluids have been examined in detail in the review of Suganthi and Rajan.[11]

Heat transfer of nanofluids flow in enclosures with obstacles, for different boundary conditions, has attracted the engagement of many research workers in recent years. Hemmat Esfe et al.[12] have examined mixed convection in a square cavity saturated with alumina-water nanofluid with a hot obstacle in the center. Their results showed that the recirculation zones grew larger with the presence of the obstacle and the addition of nanoparticles leads tohigher heat transfer rates. Rashad et al.[13] analysed MHD nanofluid heat transfer inside a cavity containing an irregular cold obstacles and filled with water-Al_2O_3 based nanofluid and the results are illustrated in terms of isotherms and streamlines. The hydrodynamic and thermal characteristics of a Newtonian fluid inside a square cold enclosure containing four interior heaters, arranged in different ways, were studied numerically by Ragui et al.[14] They found that the arrangement of the heaters in the enclosure leads to a significant improvement in heat transfer. In a recent study, Rahmati and Tahery[15] presented numerical results of the natural convection of (water-TiO_2) nanofluid in a square cavity equipped with a hot obstacle by the method Lattice Boltzmann (LBM). These authors studied the effect of the Rayleigh number, the size of the obstacle, the volume fraction of nanoparticles, the aspect ratio of the cavity and various models of the thermal conductivity, and the viscosity were used to calculate the average Nusselt number. The results show that the average Nusselt number increases with increasing Rayleigh number, volume fraction of nanoparticles and size of the obstacle surface. Thus, all results are similar for the Hamilton-Crosser model and Maxwell-Garnett, when the aspect ratio is equal to one. Garoosi and Rashidi[16] studied numerically the conjugate mixed convection of various types of nanofluid in a 2D cavity for both cases of internal/external heating and cooling, for various pertinent parameters such asRichardson number, thermal conductivity ratio, conductive obstacle, number of the hot obstacle, and volume fraction, size and type of nanoparticles. They found that at low Richardson numbers, the type and the size of the nanoparticles have a trivial impact on the Nusselt number. However, at high values of Richardson number, ultra-fine particles with elevated thermal conductivity (such as Cu, $ds = 25$ nm) provide a more increased heat transfer rate, compared to larger particles with low thermal conductivity (like TiO_2 with $ds = 145$ nm). A comprehensive review of the mixed convection of nanofluids in different forms of enclosures has been the subject of a thorough analysis by Izadi et al.[17] Their results show that the heat transfer rate enhanced with an increasein the Richardson and the Reynolds numbers, for constant nanoparticles volume fraction. In addition, the heat transfers rate increases with an increase in the nanoparticles volume fraction, at a constant Reynolds number. Mansour et al.[18] investigated time-dependent convective of nanofluids in an enclosure filled with nanofluids subjected to changeable thermal boundary conditions. It is found that an increase in the Hartmann number results in a clear reduction in the rate of heat transfer. Increasing in solid volume fraction (Cu-Water nanofuid), leads to a decrease in both the activity of the fluid motion and the fluid temperature, Ahmed et al.[19] The internal heat generating nanofluid filled cavity with several boundary conditions was investigated by Ref. [20].

The study of natural convection of nanofluids flow under the effect of an external magnetic field has attracted the attention of several researchers, because of their importance in different industrial processes, e.g., materials processing, flow and heat transfer in solar pools, dynamics of lakes, crystal growing, float-glass production, metal casting, galvanizing, and metal coating, etc.[21–23] Sadeghi et al.[24] presented a review on the studies that included the use of cavities and enclosures in different geometric shapes. The generation of thermal entropy increases by an increase in the porosity of medium due to higher friction in a fuid.

Selimefendigil and Öztop[25] numerically analyzed natural convection in a square cavity, filled with nanofluids with obstacles of different shapes (circular, square and diamond) established under the influence of a constant magnetic field and generation of a heat source. The cavity was heated from the bottom and cooled on the vertical sides, while the top wall was assumed to be adiabatic. Sidewall temperatures vary linearly. The numerical study was carried out for a range of parameters: the external and the internal Rayleigh numbers and the Hartmann number. The results obtained show that the presence of the obstacles destroys the process of heat transfer and this is more pronounced with higher values of the external Rayleigh number. The average heat transfer is reduced by 21.35%, 32.85% and 34.64% for the cavity with the circular, diamond and square obstacle, respectively. Rashad et al.[26] investigated convective heat transfer of a hybrid nanofluid filled in a triangular cavity subjected to a constant magnetic field. The hybrid nanofluid composed of equal quantities of Cu and Al_2O_3. Their results show that the increase in the volume fraction of the hybrid nanofluid is very significant when the natural convection is less important. Javed and Siddiqui[27] investigated natural convective heat transfer through a triangular cavity containing

a heated square obstacle and filled within ferrofluid, under a uniform magnetic field. It was observed that the intensification of the magnetic field weakens the strength of streamline circulations and the conduction regime became dominant, for all Hartmann numbers more particularly when the Rayleigh number is taken small. Increasing the Rayleigh number intensifies the convection currents, while isotherms become highly distorted, this shows a dominant convection regime for large Rayleigh numbers and a considerable heat transfer rate of the ferrofluid (Cobalt–water) compared to that of the base fluid. Furthermore, increasing the aspect ratio of the obstacle reduces the magnitude of streamline circulations. Ayoubloo et al.[28] theoritically investigated the free convection flow and heat transfer of a non-Newtonian fluid with pseudoplastic behavior in a cylindrical vertical cavity partially filled with a layer of a porous medium. The obtained results show that increase of pseudoplastic behavior and increase of the thickness of the porous layer enhances the heat transfer. Armaghani et al.[29] described that the Nusselt number values amplify with rising values of Rayleigh number in their work on isotherms and fluid lines analysis of nanofluid inside an I-shaped cavity. Mixed convection in a lid-driven cavity, filled with alumina nanofluid and provided with an obstacle under the action of a uniform magnetic field has been analyzed numerically by Hussain et al.[30] The results obtained demonstrate that the average Nusselt number increased when the Richardson number and the nanoparticles volume fraction increases and decreases respectivelywith the increase of the magnetic field intensity. Xiong et al.[31] performed an investigation on heat convection of alumina nanofluid, under a magnetic field influence. Their results proved that the average Nusselt number augments meaningfully with Rayleigh and Darcy numbers as well as the nanoparticles shape factor. The impact of two-phase nanofluid model on mixed convection heat transfer in a double lid-driven square cavity in the presence of amagnetic field was investigated by Ref. [32], where they showed that the heat transfer rate enhances with an increment of Reynolds number or a reduction of Hartmann number. Benzema et al.[33] examined numerically the effect of an external magnetic field on heat transfer and entropy generation of hybrid nanofluid, in a partially heated irregular ventilated cavity, for different controlling parameters. They noticed that the intensification of the magnetic field tends to attenuate the heat transfer convection and reduce the thickness of the thermal boundary layer. The addition of nanoparticles improves the heat transfer rate, for all values of Hartmann and Reynolds numbers.

The investigation of the orientation effect of the magnetic field in two cavities (2D and 3D) has attracted the attention of several numerical studies recently. Some studies were dedicated to natural convection in 3D or 2D cavities, filled with nanofluids Yu and Tian,[34] Ozoe and Okada,[35] Kefayati and Tang[36] and Al-Rashed et al.[37] They found that the angle of inclination plays a big role in the flow and heat transfer. Rashad et al.[38] discussed the consequences of size and location of heat sink/source on MHD free convection and entropy generation of nanofluids in an inclined porous cavity. The highest heat transfer was found for the inclination angles ranging from 40 to 50° or 300 to 310°. Mansour et al.[39] explored an inclined square cavity with nano-fluids and heating circular solid. They found that The magnetic field parameter, Ha, decreases the average Nusselt number, and it has the tendency to break down large size vortices into smaller ones. Mixed convection and entropy generation in a lid-driven T-shaped porous cavity in Galerkin FEM, investigated by Hussain et al.,[40] with parameters Richardson number (Ri), Darcy number (Da), angle of inclination of magnetic field (γ), aspect ratio (AR) and Hartmann number (Ha). The improvement of the heat transfer with the rising of the volume fraction of the nanoparticles was also studied by Ref. [32]. Natural convection heat transfer and fluid flow induced by a centrally located thermally active plate in the presence of an external magnetic field imposed separately, in the three directions, were investigated numerically by Purusothaman et al.[41] The results obtained show that the heat transfer rate is strongly disadvantaged by the X and Y directional magnetic field, and this influence is less noticeable in the Z direction. In addition, heat transfer becomes more improved for the vertical plate compared to the horizontal plate, and as the aspect ratio of the heated plate increases, the mean Nusselt number increases. Sheikholeslami et al.[42] investigated magneto-convective flow of water-based nanofluids in a porous cubic cavity, with a hot sphere obstacle, taking into account Brownian motion. Their results show that the Lorentz forces decrease the temperature gradient. The thermal boundary layer becomes then wider with the increase of Hartmann number. The effects of an outward-facing magnetic field and different thermal boundary conditions on MHD natural convection in a saturated porous medium with a nanofluid-filled cavity, have been studied numerically by Rashad et al.[43] Their results show a good improvement in average Nusselt number can be obtained by increasing the nanoparticle volume fraction.

Jelodari and Nikseresht[44] studied the effects of the Lorentz force and the generated electrical field on the thermal performance of magnetic Seawater–Aluminum oxide nanofluid filled cubic cavity, for different controls parameters such as Rayleigh number, nanoparticles volume fraction, Lorentz force and applied magnetic field direction. They found that imposing magnetic field along X direction has a very important effecton the heat transfer rate. Indeed, for higher Rayleigh number values, the Lorentz force has no notable effect.

The comparison between 2D and 3D models in the existence of a magnetic field was one of the purposes of Zhang et al.[45] They found that the differences in flow and temperature distribution, between 2D cavity and 3D cavity (on

the middle *XY*-plane in the spanwise direction) are excellent for high level thermal radiation and weak magnetic field, and become smaller for weaker thermal radiation and stronger magnetic field. Recently, Kherroubi et al.[46] investigated the effect of the Lorentz force and the outlet positions, for different control parameters, in mixed convection of a nanofluid. Their results reveal that the three-dimensional flow maintains the behavior of the two-dimensional flow to relatively higher values of the Lorentz force and the heat transfer rate depends on the outlet position.

It can be seen, in the literature, that most of the previous researches were limited to two-dimensional geometries, due to the difficulty of 3D flows simulation. Therefore, to simulate more real flow, numerical simulations of three-dimensional geometry are necessary. The main aim of this study is to study the MHD flow and heat transfer in a cubic cavity filled with TiO_2-Water-Nanofluid, with a hot block inside, for various parameters such as; the Rayleigh number, the inclination angle of the magnetic field, for different Hartmann numbers, as well as the nanoparticles volume fraction have been considered. Thus, the comparison between the two models (two-dimensional and three-dimensional) for different governing parameters has been undertaken, in order to show the third direction effect on the magnetohydrodynamic behavior of the nanofluid flow. Titanium dioxide (TiO_2) is one of promising materials for heat transfer enhancement purpose due to its excellent chemical and physical stability. In addition, TiO_2 particles are cheap and commercially available. TiO_2 nanoparticles suspended in conventional fluids were extensively utilized in various forms of heat exchangers.

2. PROBLEM DESCRIPTION AND MATHEMATIC FORMULATION

2.1. Problem Configuration

The geometry studied in this work is a cubic cavity (length L, height H and width W) completely filled with a nanofluid (TiO_2-water), having a hot block, centered of dimension (0.2 H, 0.2 L and W). The vertical walls (Left and Right) are cold isotherms; the bottom wall is kept hot while the top wall and the side walls (rear wall, front wall) are adiabatic. The natural convection flow, which develops in the enclosure, is exposed to an external uniform magnetic field, of intensity B_0 oriented with an angle ω with respect to the horizontal axis *OX* (Fig. 1(a)). Figure 2(b) represents the square geometry in the case where the cubic cavity is very long along the third direction *OZ*. No-slip and impermeability boundary conditions are imposed on the walls of the cavities and on the surface of the hot block.

In this study, the flow is assumed to be laminar and the nanofluid incompressible. The induced magnetic field, generated by the motion of an electrically conducting nanofluid, is assumed to be negligible as compared to the applied magnetic field. Moreover, the Hall Effect is assumed negligible. The base fluid and solid nanoparticles are in thermal equilibrium. Slipping effect between any two phases, radiation effects and viscous dissipation in the energy equation are neglected. The standard Boussinesq model is used to model the density in the buoyancy term.[15, 36, 45] The other thermo-physical properties of the nanofluid are assumed constant (See Table I).

2.2. Governing Equations

When the magnetic field exists, the non-dimensional governing equations for 2D and 3D MHD flow and heat transfer can be written as follows:[46–48, 50]

$$\nabla \cdot \vec{V}' = 0 \tag{1}$$

$$\rho_{nf}\left(\vec{V}' \cdot \nabla\right)\vec{V}' = -\nabla p + \mu_{nf}\nabla^2\vec{V}' + (\rho\beta)_{nf}\left(T - T_C\right)\vec{g} + \vec{F} \tag{2}$$

$$\vec{V}' \cdot \nabla T = \alpha_{nf}\nabla^2 T \tag{3}$$

Where the applied magnetic field B ($\vec{B} = \vec{B}_x\vec{i} + \vec{B}_y\vec{j} + \vec{B}_z\vec{k}$) is uniform with a constant magnitude:

$$B_0\left(B_0 = \sqrt{B_x^2 + B_y^2 + B_z^2}\right)$$

The interaction between the electromagnetic fields and the electrically-conducting fluid flow constitutes the Lorentz force:[34, 36, 49]

$$\vec{F} = \vec{J} \wedge \vec{B} \tag{4}$$

The electric current density *J* is computed according to the Ohm's law in the case where the strength of Coulomb is unimportant.[34, 36]

$$\vec{J} = \sigma_{nf}\left[\vec{E} + \left(\vec{V}' \wedge \vec{B}\right)\right] \tag{5}$$

Where (σ_{nf}) is the electrical conductivity of nanofluid, ($\vec{E}$) is the electric field intensity.

When the all walls of the cavity are electrically insulated:[34]

$\vec{E} = 0$

Where V' ($\vec{V}' = u\vec{i} + v\vec{j} + w\vec{k}$) is velocity vector. So, the expressions of the Lorentz force components are defined for *x*, *y* and *z* directions, respectively:

$$\begin{cases} F_x = -\sigma_{nf} B_0^2 \sin\omega\,(u\sin\omega - v\cos\omega) \\ F_y = -\sigma_{nf} B_0^2 \cos\omega\,(v\cos\omega - u\sin\omega) \\ F_z = -\sigma_{nf} B_0^2\, w \end{cases} \tag{6}$$

The effective density, heat capacity and thermal expansion coefficient of the nanofluid are as following, respectively.[50]

$$\rho_{nf} = (1-\varphi)\,\rho_{bf} + \varphi\,\rho_s \tag{7}$$

$$\left(\rho C_p\right)_{nf} = (1-\varphi)\left(\rho C_p\right)_{bf} + \varphi\left(\rho C_p\right)_s \tag{8}$$

$$(\rho\beta)_{nf} = (1-\varphi)\,(\rho\beta)_{bf} + \varphi\,(\rho\beta)_s \tag{9}$$

ARTICLE

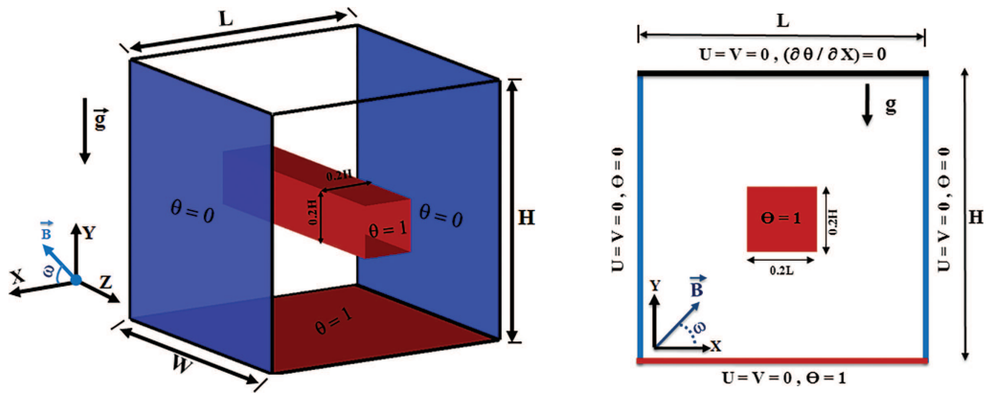

(a) (b)

Fig. 1. Geometrical description of the physical problemwith boundary conditions: (a) 3D configuration, (b) 2D configuration.

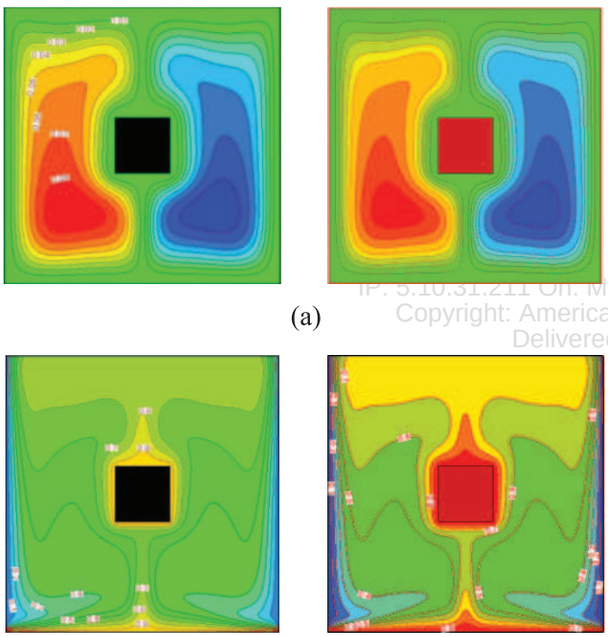

(a)

(b)

Rahmati et *al.*[15] Present work

Fig. 2. Comparison with Rahmati et al.[15] results. Ra = 10^6; $\varphi = 4\%$. (a) Streamlines. (b) Isotherms.

The dynamic viscosity and thermal conductivity of the nanofluid can be estimated by the following empirical correlations produced by Corcione.[51] These correlations are obtained by a large number of experimental data, reported in the literature by various research teams, whose standard deviation of error is 1.86%.[52]

$$\frac{\mu_{nf}}{\mu_{bf}} = \frac{1}{1 - 34.87\left(d_s / d_{bf}\right)^{-0.3} \varphi^{1.03}} \tag{10}$$

$$\frac{k_{nf}}{k_{bf}} = 1 + 4.4\,\mathrm{Re}_s^{0.4}\,\mathrm{Pr}^{0.66}\left(T / T_{fr}\right)^{10}\left(k_s / k_{bf}\right)^{0.03}\varphi^{0.66} \tag{11}$$

Table I. Thermophysical properties of water and TiO_2 nanoparticles.[5]

	Cp (J kg^{-1} K^{-1})	ρ (kgm^3)	k (W m^{-1} K^{-1})	β (K^{-1}) × 10^5
H_2O	4179	997.1	0.613	21
TiO_2	686.2	4250	8.9538	0.9

Where $d_s = 25$ nm is the diameter of TiO_2 nanoparticles,[51,53] $d_{bf} = 0.3854$ nm is the equivalent diameter of a base fluid molecule (Water), determined by Eq. (13) at the reference temperature $T_C = 293.15$ K, Re_s is the nanofluid particle Reynolds number, taken into the hypothesis that Brownian diffusion and thermosphere's are the primary slip mechanisms between solid and liquid phases, calculated by Eq. (12). $\kappa_B \approx 1.38 \times 10^{-23}$ J/K; is the Boltzmann's constant, and $T_{fr} = 273.15$ K, $M = 18.01528$ g/mol and $\mu_{bf} = 1.003 \times 10^{-3}$ kg/ms are the freezing point, molar mass and dynamic viscosity, respectively of the base fluid, while $N = 6.022 \times 10^{23}$ molecules/mol is the Avogadro number.

$$\mathrm{Re}_s = \frac{2\,\rho_{bf}\,\kappa_B\,T}{\pi\,\mu_{bf}^2\,d_s} \tag{12}$$

$$d_{bf} = \left(\frac{6\,M}{N\,\pi\,\rho_{bf}}\right)^{1/3} \tag{13}$$

The dimensionless form of the governing equations can be given as follows:

$$(X,\,Y,\,Z) = \frac{(x,\,y,\,z)}{H}; \quad (U,\,V,\,W) = \frac{(u,\,v,\,w)}{\left(\alpha_{bf}/H\right)};$$

$$\theta = \frac{T - T_C}{T_H - T_C} \quad P = \frac{p\,L^2}{\rho_{bf}\,\alpha_{bf}^2}; \quad \mathrm{Pr} = \frac{\nu_{bf}}{\alpha_{bf}};$$

$$Ra = \frac{g\,\beta_{bf}\,(T_H - T_C)\,H^3}{\alpha_{bf}\,\nu_{bf}}; \quad Ha = B_0\,L\left(\frac{\sigma_{nf}}{\mu_{bf}}\right)^{1/2} \tag{14}$$

After substitution of the above variables, we get the following dimensionless equations:[54, 55]

$$\frac{\partial U}{\partial X}+\frac{\partial V}{\partial Y}+\frac{\partial W}{\partial Z}=0 \tag{15}$$

$$U\frac{\partial U}{\partial X}+V\frac{\partial U}{\partial Y}+W\frac{\partial U}{\partial Z}=-\frac{\partial P}{\partial X}+\frac{\mu_{nf}}{\rho_{nf}\,\alpha_{bf}}\left(\frac{\partial^2 U}{\partial X^2}+\frac{\partial^2 U}{\partial Y^2}+\frac{\partial^2 U}{\partial Z^2}\right)-\mathrm{Pr}\,Ha^2\sin\omega\times(U\sin\omega-V\cos\omega) \tag{16}$$

$$U\frac{\partial V}{\partial X}+V\frac{\partial V}{\partial Y}+W\frac{\partial V}{\partial Z}=-\frac{\partial P}{\partial Y}+\frac{\mu_{nf}}{\rho_{nf}\,\alpha_{bf}}\left(\frac{\partial^2 V}{\partial X^2}+\frac{\partial^2 V}{\partial Y^2}+\frac{\partial^2 V}{\partial Z^2}\right)+\frac{(\rho\beta)_{nf}}{\rho_{nf}\,\beta_{bf}}Ra\,\mathrm{Pr}\,\theta-\mathrm{Pr}\times Ha^2\cos\omega\,(V\cos\omega-U\sin\omega) \tag{17}$$

$$U\frac{\partial W}{\partial X}+V\frac{\partial W}{\partial Y}+W\frac{\partial W}{\partial Z}=-\frac{\partial P}{\partial Z}+\frac{\mu_{nf}}{\rho_{nf}\,\alpha_{bf}}\left(\frac{\partial^2 W}{\partial X^2}+\frac{\partial^2 W}{\partial Y^2}+\frac{\partial^2 W}{\partial Z^2}\right)-\mathrm{Pr}\,Ha^2 W\times\left(\cos\omega^2+\sin\omega^2\right) \tag{18}$$

$$U\frac{\partial\theta}{\partial X}+V\frac{\partial\theta}{\partial Y}+W\frac{\partial\theta}{\partial Z}=\frac{\alpha_{nf}}{\alpha_{bf}}\left(\frac{\partial^2\theta}{\partial X^2}+\frac{\partial^2\theta}{\partial Y^2}+\frac{\partial^2\theta}{\partial Z^2}\right) \tag{19}$$

Where $\alpha_{nf}=k_{nf}/\left(\rho\,C_p\right)_{nf}$

2.3. Heat Transfer Characteristics

The local and average Nusselt numbers at the cold walls are determined as:

$$Nu=\left(-\frac{k_{nf}}{k_{bf}}\right)\frac{\partial\theta}{\partial X}\bigg|_{\mathrm{wall}} \tag{20}$$

$$Nu_{\mathrm{avg}}^{2D}=\frac{1}{2H}\left(\int_0^H Nu|_{X=0}\,dy+\int_0^H Nu|_{X=L}\,dy\right) \tag{21}$$

$$Nu_{\mathrm{avg}}^{3D}=\frac{1}{2\,H\,W}\left(\int_0^W\int_0^H Nu|_{X=0}\,dy\,dz+\int_0^W\int_0^H Nu|_{X=L}\,dy\,dz\right) \tag{22}$$

The normalized average Nusselt number for 2D or 3D is defined as the ratio of Nusselt number, for $\varphi=5\%$ to that of pure fluid $\varphi=0\%$:

$$Nu^*(Ha,\,\omega)=\frac{Nu_{\mathrm{avg}}(\varphi=5\%)}{Nu_{\mathrm{avg}}(\varphi=0\%)} \tag{23}$$

The performance advantage of nanoparticles is determined by calculating the ratio between the case in which the magnetic field is present and the case without the magnetic field, for a constant value of the volume fraction of the nanoparticle ($\varphi=5\%$) and Hartmann number, $Ha=90$:

$$CM=\frac{Nu^*_{\mathrm{Avg}}(\varphi=5\%,\,Ha=90)}{Nu^*_{\mathrm{Avg}}(\varphi=5\%,\,Ha=0)} \tag{24}$$

3. BOUNDARY CONDITIONS

The dimensionless boundary conditions can be mathematically expressed as follows. The adopted hydrodynamic boundary conditions for all walls and surface block are:

- U = V = W = 0

The adopted thermal boundary conditions are:

- Cold walls: $\theta=0$
- Hot wall: $\theta=1$
- Adiabatic wall: $(\partial\theta/\partial Y)|_{Y=1}=0$
- Solid hot block: $\theta=1$

4. NUMERICAL PROCEDURE, GRID DEPENDENCY AND CODE VALIDATION

4.1. Numerical Procedure

The non dimensional governing equations Eqs. (15)–(19) with boundary conditions were solved by finite volume method using the uniform grid for all directions. The SIMPLER Algorithm of Patankar[56] was applied to solve the velocity-pressure coupling. The power law scheme is applied for convective terms and central difference scheme for diffusion terms. The algebraic equations were solved by the line-by-line procedure, combining the Tridiagonal Matrix Algorithm (TDMA).

The numerical simulations were accomplished thanks to the executions made by a 3-D calculation code, using a personal microcomputer, Pentium i5 with a frequency of 2.53 GH and a RAM equal to 4 GB. The calculation time required for the convergence of a single execution reaches 3 hours 30 min.

The convergence condition used for this study is:

$$\frac{\sum_{k=1}^{N}\sum_{j=1}^{M}\sum_{i=1}^{L}\left|\phi_{i,j,k}^{\xi+1}-\phi_{i,j,k}^{\xi}\right|}{\sum_{k=1}^{N}\sum_{j=1}^{M}\sum_{i=1}^{L}\left|\phi_{i,j,k}^{\xi+1}\right|}\le 10^{-5} \tag{25}$$

where L, M, and N are the numbers of grid points in X-, Y- and Z-directions, respectively,ϕ is any of the computed field variables and ξ is the iteration number.

4.2. Code Validation

Firstly, the quantitative verification of the present code for free convection in a cubical cavity was performed, by a comparison of the present results with the three-numerical simulation, reported by Ozoe and Okada,[35] who

ARTICLE

Table II. Comparison of the present results with those obtained by Javed and Siddiqui.[27]

	Nu^{3D}_{avg}	
	Present work	Vanaki et al.[10]
$Ha = 100$	4.439	4.457
$Ha = 200$	2.892	2.917

studied the influence of the external magnetic field direction on the heat transfer and flow structure. A comparison of the results for a magnetic field in the X-direction for ($\mathrm{Pr} = 0.054$, $\mathrm{Ra} = 10^6$), and two values of Hartmann number ($\mathrm{Ha} = 100$ and $\mathrm{Ha} = 200$), is shown in Table II. The present results are in good agreement with past research.

Secondly, for the two-dimensional cavity, a qualitative verification was conducted by comparing flow structures and isotherms with those obtained by Rahmati and Tahery,[15] for the case of $\mathrm{Ra} = 10^6$ and the presence of nanoparticles $\varphi = 4\%$ (Fig. 2). Again, with the application of a horizontal magnetic field ($\omega = 0°$), we qualitatively compare isotherms obtained by our code with the results of Yu et al.[57] in Figure 3 for two cases ($\mathrm{Ra} = 10^4$, $\mathrm{Ha} = 100$ and $\mathrm{Ra} = 10^5$, $\mathrm{Ha} = 30$). The results show very good similitude.

Finally, the temperature distributions along the horizontal median line ($Y = 0.50$) were compared with the experimental results of Krane[58] and the numerical results of Khanafer et al.[59] (Fig. 4). Moreover, in order to ensure the relevance of the Corcione correlations (for the dynamic viscosity and the thermal conductivity of the nanofluids) in the house code, we also compared our results with those of Ternik[60] in terms of temperature distribution along the longitudinal axis (OX), in $Z = 0.50$, within a cubic cavity, differentially heated and filled with a nanofluid (Au-water) at 5% (Fig. 5). The result of these two comparisons shows good agreement with the Refs. [58–60].

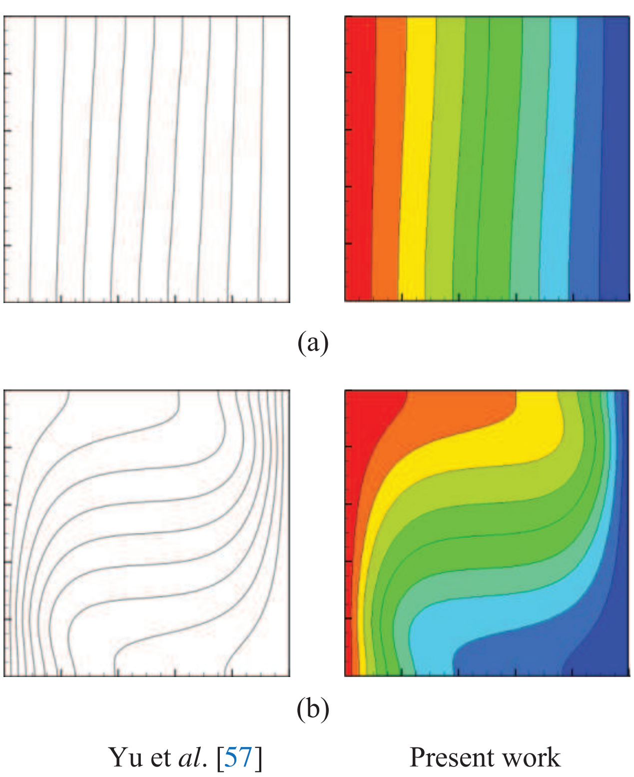

Fig. 3. Comparison of isotherms between the present work and that of Yu et al.[57] $\omega = 0°$: (a) $Ra = 10^4$; $Ha = 100$. (b) $Ra = 10^5$; $Ha = 30$.

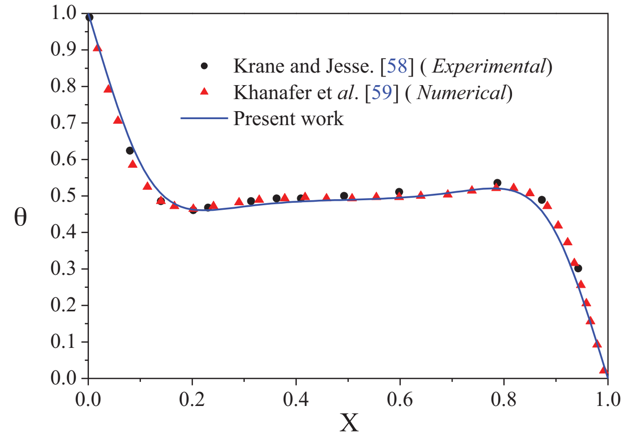

Fig. 4. Comparison of the temperature distribution with experimental results[58] and numerical results.[59] $Ra = 1.89 \times 10^5$; $Pr = 0.71$.

4.3. Grid Dependency

In order to choose the appropriate grid size for both configurations (2D and 3D), a grid sensitivity was achieved, in terms of the variation of the average Nusselt number calculated on the cold walls for $Ra = 10^6$, $Ha = 45$ and $\varphi = 5\%$ and inclination angle of the magnetic field ($\omega = 45°$), using different grids as shown in Tables III and IV, respectively. We observe that the grid independence for the 2D model is 300^2 and 71^3 for the 3D model.

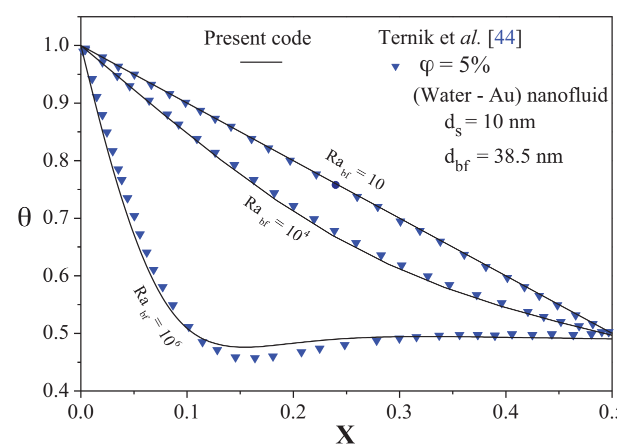

Fig. 5. Comparison of non-dimensional temperature along the centerline of the cubic cavity using Corcionne correlation for (water-Au) nanofluid.

Table III. Grid sensitivity analysis for 2D configuration. $Ra = 10^6$; $\omega = 45°$; $Ha = 90$; $\varphi = 5\%$.

Grid size (ψ)	Nu_{avg}^{2D}	$\Delta(\%) = \frac{Nu_{Avg}(\psi) - Nu_{Avg}(\psi-1)}{Nu_{Avg}(\psi-1)} \times 100$
200^2	10.8608	
220^2	10.9253	0.5938
240^2	10.9901	0.5931
260^2	11.0420	0.4722
280^2	11,0959	0.4881
300^2	11.1432	0.4262

Table IV. Grid sensitivity analysis for 3D configuration. $Ra = 10^6$; $\omega = 45°$; $Ha = 90$; $\varphi = 5\%$.

Grid size (ψ)	Nu_{avg}^{3D}	$\Delta(\%) = \frac{Nu_{Avg}(\psi) - Nu_{Avg}(\psi-1)}{Nu_{Avg}(\psi-1)} \times 100$
50^3		
56^3	10,0149	
60^3	10.0158	0.0089
64^3	10.0182	0.0234
68^3	10.0203	0.0209
72^3	10.0225	0.0219
76^3	10.0243	0.0179

5. RESULTS AND DISCUSSION

In this part, we numerically analyze, in natural convection mode, the flow of a nanofluid within cavities (square and cubic), for different control parameters, namely Rayleigh number, Hartmann number, inclination angle of the magnetic field and nanoparticles volume fraction. The results are presented in terms of thermo-hydrodynamic structures, velocity profiles, average Nusselt number and nanoparticle merit coefficient, as well as a qualitative and quantitative comparison between the two-dimensional model and the three-dimensional model.

5.1. Thermohydrodynamic Field Structure

In the absence of the magnetic field, Figures 6 and 7 represent the hydrodynamic structure (streamlines) and thermal structure (isotherms) of water-TiO_2 nanofluid versus Rayleigh numbers and nanoparticles volume fraction ($\varphi = 0\%$; $\varphi = 5\%$) for the 3D configuration in three (X–Y) planes ($Z = 0.05$, $Z = 0.50$ and $Z = 0.95$) and 2D configuration.

Firstly, the results obtained for the 3D configuration (Fig. 6) illustrate that the main flow is described by two counter-rotating vortices. The fluid layers adjacent to the hot block and to the lower wall undergo heating and see their density decrease, which gives them an upward movement, while the fluid layers in contact with the cold vertical walls are subjected to cooling, which borrow the fluid a descending movement. As a result, the left vortex of the cavity rotates counterclockwise, while the right vortex rotates clockwise. In addition, it is seen that by increasing the Rayleigh number, streamlines become closer to cavity boundary layers, and this is more clear for larger Rayleigh numbers ($Ra = 10^6$). It is worth noting that the shape of rotating vortices of the 3D configuration is spiral, while those corresponding to the 2D configuration are closed and have a larger size, given the fact that side walls effect has been eliminated. Secondly, we note that the structure of the streamlines in the three planes is almost identical, as long as the Rayleigh number is less than 10^4. On the other hand, for higher Rayleigh numbers ($Ra \leq 10^5$), the effect of the front and rear walls is important and cannot be neglected, and the similarity observed previously is not retained. However, for the cases $Z = 0.05$ and $Z = 0.95$, a symmetry with respect to the median plane ($Z = 0.50$) is observed, characterized by a less developed flow structure in comparison with that corresponding to $Z = 0.50$, which escapes the influence of the adiabatic walls. Concerning nanoparticles effect on the streamlines, it does not make a big effect on flow distribution.

Isothermal structures are shown in the Figure 7, where it can be seen, for $Ra = 103$ and 104, that the hot fluid is trapped between the lower wall of the cavity and that of the hot block, given the low intensity of the buoyancy forces, while isotherms are parallel to the cold vertical wall, denoting a conductive heat transfer.

On the other hand, when Ra becomes larger ($Ra > 10^5$), the convection currents impose themselves inside the cavity, giving rise to a strong curvature of the isotherms. Also, the evacuated heat is able to propagate towards the upper parts of the cavity. We can also observe that the thickness of the thermal boundary layer along the hot block and the left, the right and the bottom walls becomes thinner with increasing Rayleigh number, which suggests a probable improvement in heat transfer. In addition, the presence of nanoparticles actually decreases the thickness of the thermal boundary layer as long as the Rayleigh number is less than or equal to 10^4, indicating an improvement in heat exchange. Nevertheless, the addition of nanoparticles is almost negligible for $Ra \geq 10^5$.

Through Figure 6, we can also compare the 2D and 3D configurations in terms of hydrodynamic and thermal field structures as a function of the buoyancy force (Ra) intensity and the presence/absence of nanoparticles (φ). Indeed, for $Ra \leq 10^4$, we can see that the streamlines structure on the middle (X–Y) plane (at $Z = 0.50$) in the 3D configuration and streamlines structure in the 2D configuration are similar, while slight differences exist. The flow intensity in the 2D cavity is greater than that in the middle (X–Y) plane in the 3D cavity, given that the adiabatic no-slip front wall ($Z = 1$) and the rear wall ($Z = 0$) hinder the inner flow in the 3D cavity. Moreover, the flow structure differences between 2D and 3D are evident for higher Rayleigh number $Ra \geq 10^5$, since the shear rate becomes important by increasing buoyancy forces. In addition, using nanofluids does not significantly modify the structure behavior as compared to pure water.

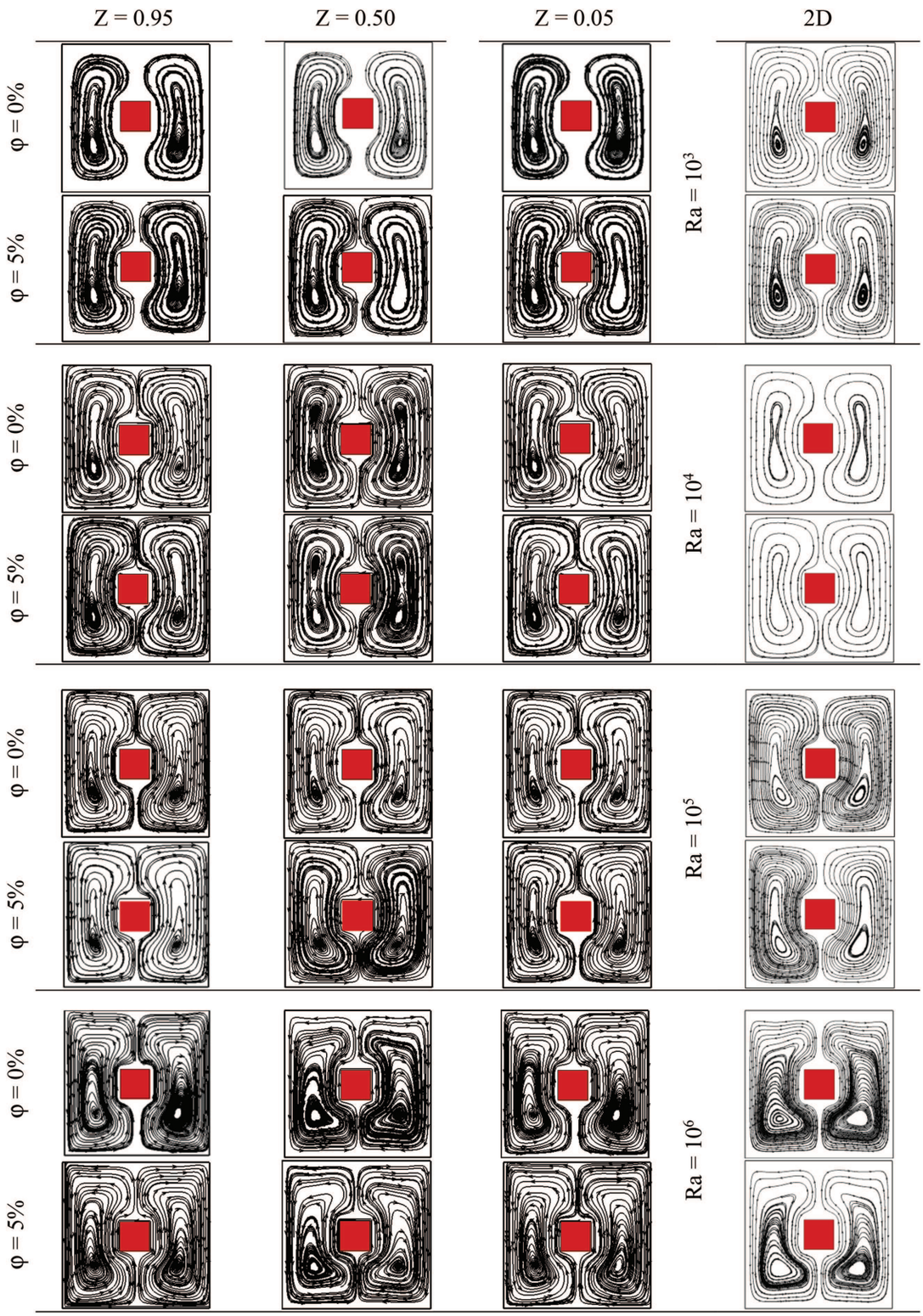

Fig. 6. Effect of Rayleigh number on the streamlines projection for the 3D configuration in the (X–Y) planes ($Z = 0.05$, $Z = 0.50$ and $Z = 0.95$) and 2D configuration. $\varphi = 0\%$; $\varphi = 5\%$.

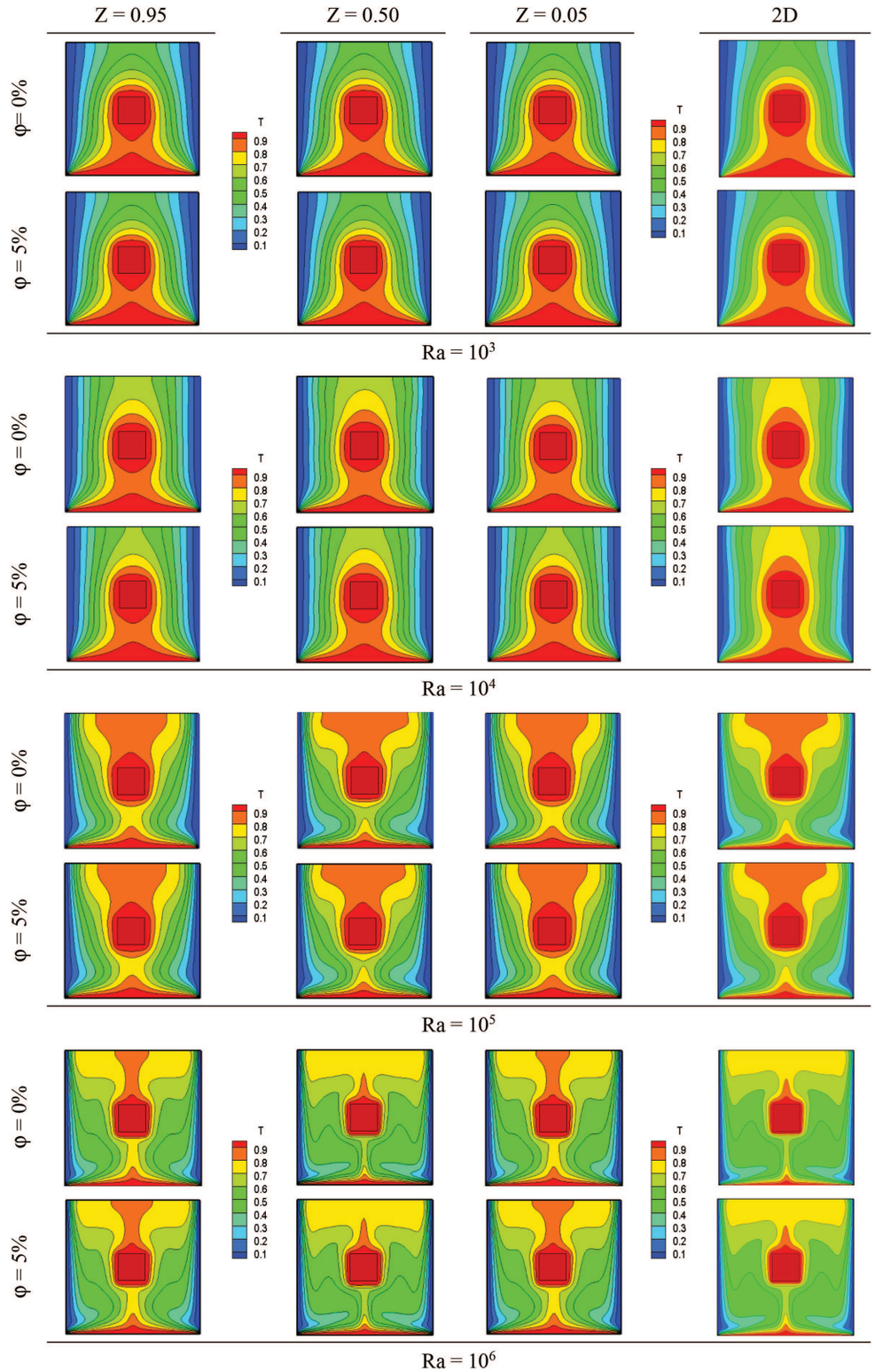

Fig. 7. Effect of Rayleigh number on the isotherms for the 3D configuration in the (Y–Z) planes ($Z = 0.05$, $Z = 0.50$ and $Z = 0.95$) and 2D configuration. $\varphi = 0\%$; $\varphi = 5\%$.

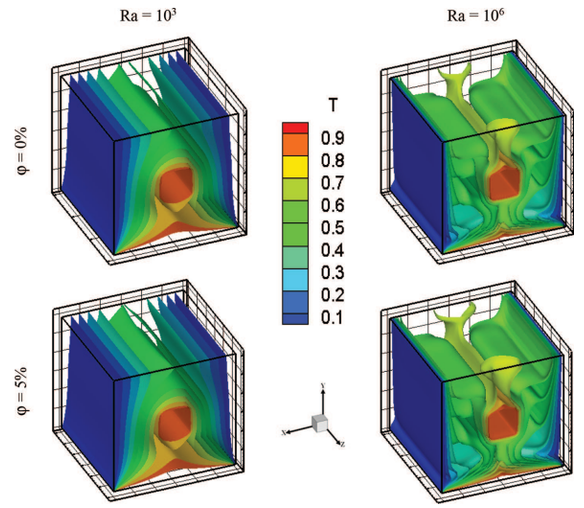

Fig. 8. Temperature isosurfaces versus Rayleigh numbers and nanoparticles volume fraction for the cubic configuration in absence of magnetic field.

Again, for isotherms structure comparison between 3D (at $Z = 0.50$) and 2D configurations, Figure 7 shows that the convection currents are more pronounced in 2D, regions with uniform temperature, different from those observed in 3D, for which, of appears a new region at a higher temperature. Moreover, there is a noticeable difference in the shape of the isotherms, particularly, in the central region of the two cavities, more precisely above and below the hot block, with the increase in the Rayleigh number. It could be concluded that the three-dimensional flow is far from being considered a two-dimensional flow whatever the value of Rayleigh number and nanoparticles fraction volume.

In order to visualize the three-dimensional distribution of the thermal and hydrodynamic field within the cubic cavity, without magnetic field, we present through Figures 8 and 9 the temperature and velocity iso-surfaces, for different control parameters.

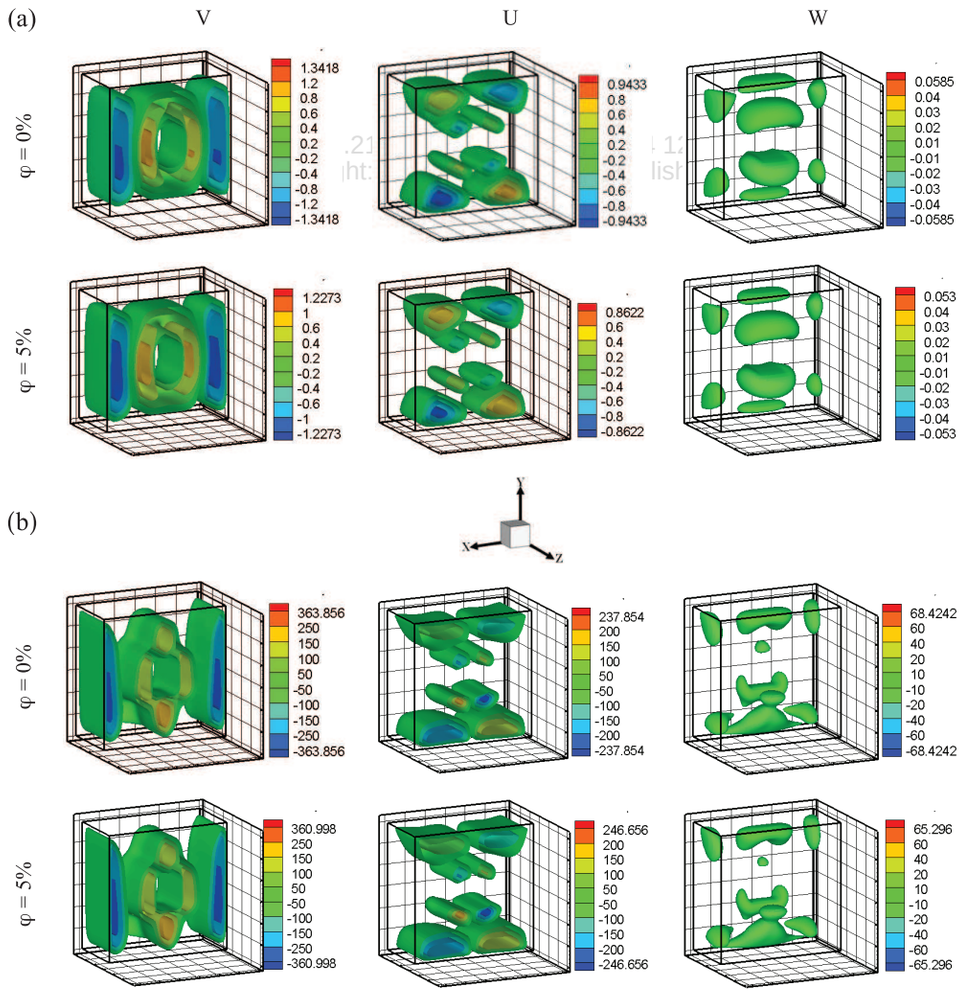

Fig. 9. Velocity isosurfaces (V, U and W) versus Rayleigh number for two values of nanoparticles volume fraction in absence of magnetic field.

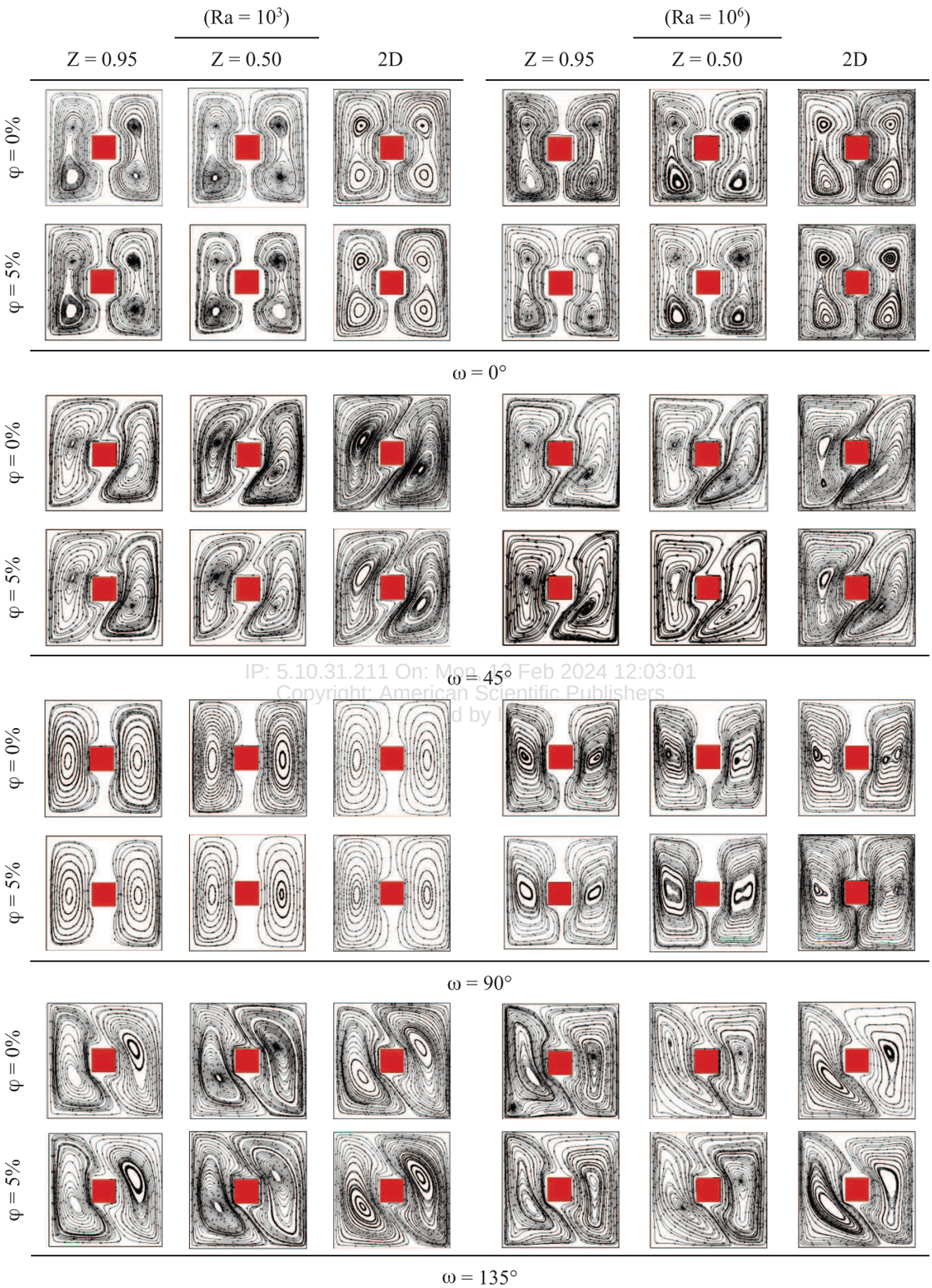

Fig. 10. Effect of inclination angles of the magnetic field and Rayleigh numbers on the streamlines for 3D configuration in the (X–Y) planes ($Z = 0.50$; $Z = 0.95$) and 2D configuration. $\varphi = 0\%$; $\varphi = 5\%$; $Ha = 90$.

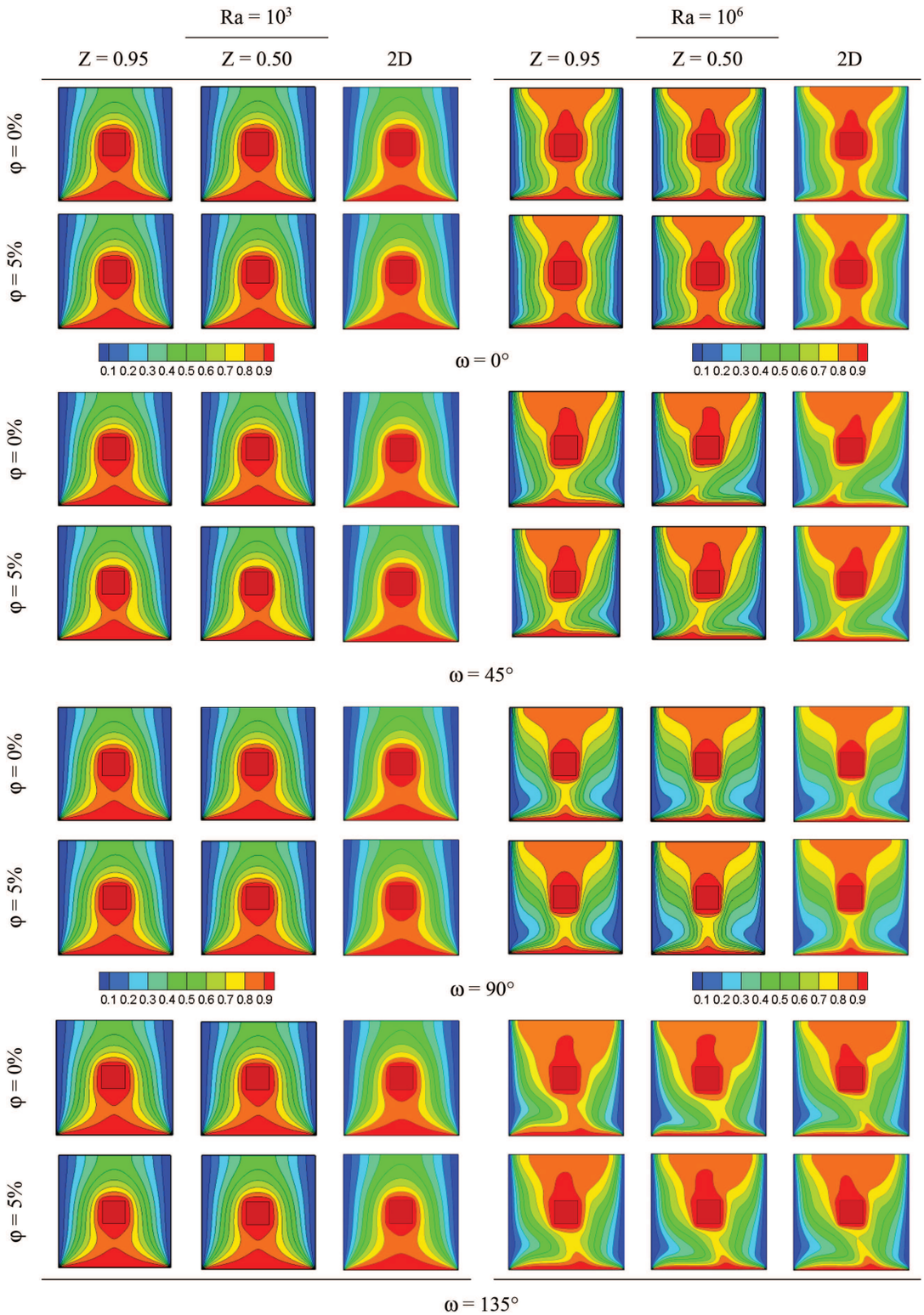

Fig. 11. Effect of inclination angles of the magnetic field and Rayleigh numbers on the isotherms for 3D configuration in the (X–Y) planes ($Z = 0.50$, $Z = 0.95$) and 2D configuration. $\varphi = 0\%$; $\varphi = 5\%$; $Ha = 90$.

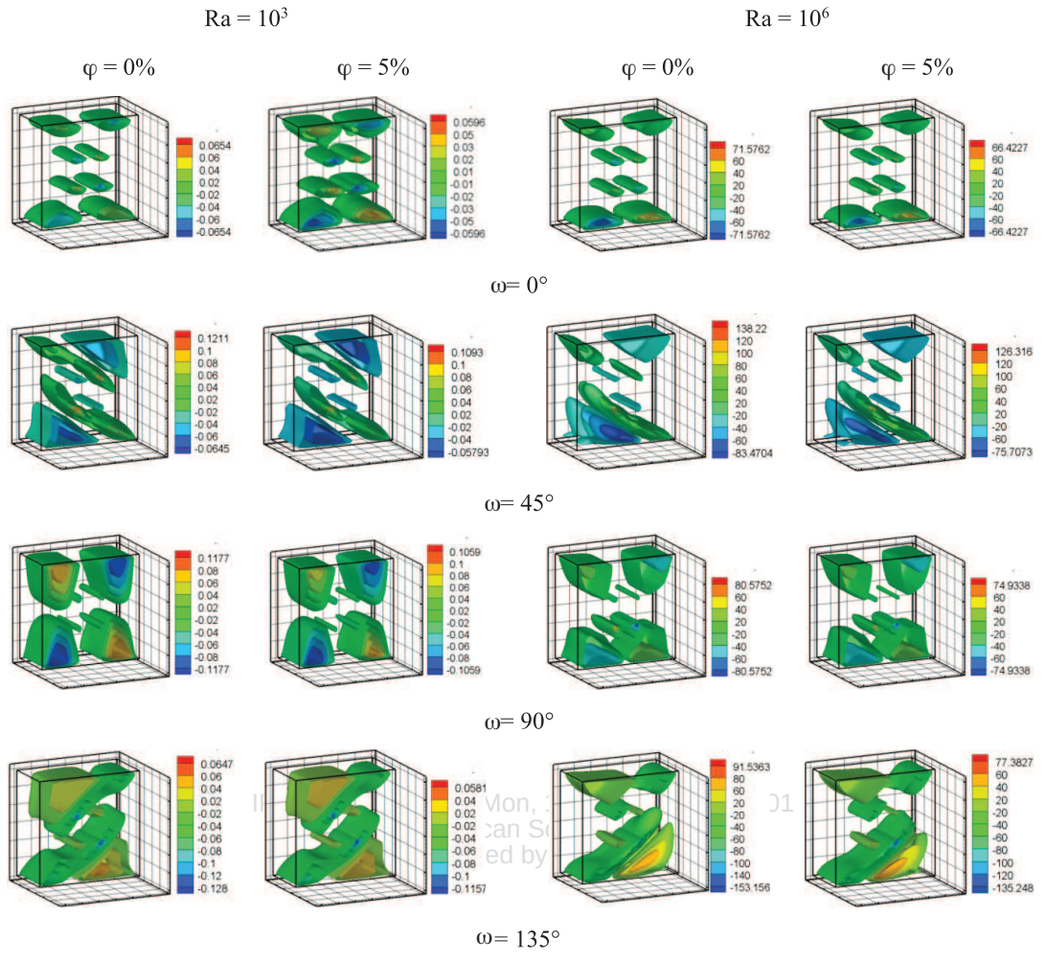

Fig. 12. Effect of inclination angles of magnetic field versus Rayleigh number and volume fraction of nanoparticles on *U*-velocity component isosurfaces.

Figure 8 shows temperature iso-surfaces for two Rayleigh numbers ($Ra = 10^3$ and $Ra = 10^6$), in the presence and in the absence of nanoparticles. For $Ra = 10^3$, a uniformly distributed stratification is observed in the central region, where the iso-surfaces are nearly parallel to the left and right cold walls, meaning that the heat transfer follows a 2D configuration. Indeed, since the front and rear walls are adiabatic, their effects are restricted to the viscous effect, which tends only to hold the fluid close to the walls. Furthermore, the addition of nanoparticles is less visible except near the adiabatic upper wall, where the temperatures of the iso-surfaces start to get closer. For $Ra = 10^6$, we note that the temperature iso-surfaces change significantly and become more curved due to the increase of the convection effect. They start to collide and tend to mix near the block. This is due to the presence of strong recirculation due to the increase in buoyancy force intensity. In the presence of 5% of nanoparticles, we notice only a small change in the size of the iso-surfaces at the level of the upper part. Moreover, we note that the thermal boundary layer thickness is significantly reduced with increasing Rayleigh number.

Figure 9 visualizes the velocity iso-surfaces (*V*, *U* and *W*) versus the Rayleigh number, only in half of the cubic cavity because of the symmetry of the problem in the *OZ* direction, as shown previously. We observe that the vertical velocity structure *V* is characterized by five rotating cells: one cell located near each cold wall and another main one, around the hot block, including two small cells, to the left and the right of the block. The structure of longitudinal velocity *U* is characterized by eight rotating cells, four main cells located at the four corners of the cavity and four medium-sized cells, around the block, at the top and in downstairs. Horizontal velocity *W* presents cells adjacent to the adiabatic wall. In addition, the figure shows also that the magnitude of these velocities increases with increasing Rayleigh number, so the magnitude of the velocity *W* is less important compared with the velocity *U* and *V*. On the other hand, the addition of nanoparticles decreases the magnitude of

ARTICLE

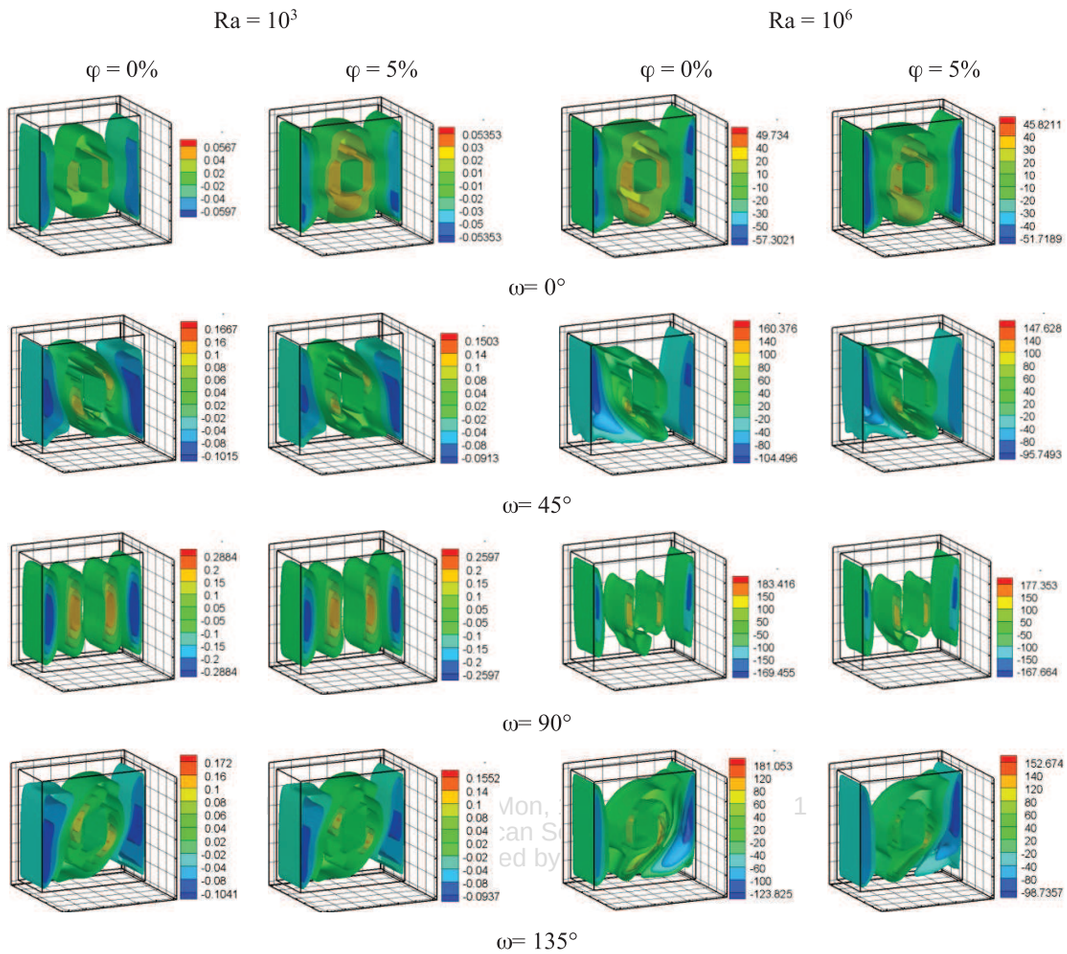

Fig. 13. Effect of inclination angles of magnetic field versus Rayleigh number and volume fraction of nanoparticles on *V*-velocity component isosurfaces.

these velocities, except in the case $Ra = 10^6$, where the magnitude of the velocity U increases with the addition of nanoparticles.

It is interesting to note finally, the multiplication of the rotating cells within the main one, for the case of the vertical velocity V, when $Ra = 10^6$.

5.2. Magneto-Thermohydrodynamic Field Structure

Figure 10 shows the hydrodynamic behavior in the presence of a magnetic field ($Ha = 90$), for two values of the Rayleigh numbers ($Ra = 10^3$ and $Ra = 10^6$) and for different inclination angles of magnetic field, in presence and absence of nanoparticles. For the 2D and 3D configurations at two planes ($Z = 0.50$ and $Z = 0.05$), the streamlines form, as previously ($Ha = 0$), two counter-rotating vortices. The symmetry is observed for $\omega = 0°$ and $\omega = 90°$ (due to the symmetry of the boundary conditions) with a decrease in the recirculation intensity, given the presence of the Lorenz force, which slows the flow within the cavity. However, for $\omega = 45°$ and $\omega = 135°$, the symmetry observed previously is destroyed. Thus, for $\omega = 45°$ one observes a spreading of the vortex on the left side of the cavity, in its upper part and on the right side, in its lower part, while for $w = 135°$, it is the reverse which occurs. This phenomenon is clearly highlighted by the important values of the Rayleigh number. In addition, sizes vortices sizes increase with increasing the Rayleigh number. Again, the presence of nanoparticles has an effect similar to that observed in the absence of a magnetic field ($Ha = 0$).

Concerning the comparison between the configurations (3D and 2D), the previous figure shows that, when the inclination angle is equal to 0° or 90°, the similarity between the streamlines structure of the middle plane ($Z = 0.50$) in the cubic cavity and in the square cavity is almost identical, compared to the case without magnetic field. This is due to the dominance of conductive regime by the combined effect of Lorentz and buoyancy forces. Or, it is because the MHD flow is suppressed, and the no-slip boundary effects of the front and rear walls are also removed. On the other hand, for the orthogonal angles (45° and 135°), the difference between the two models is considerable; this difference is due to high viscous effects

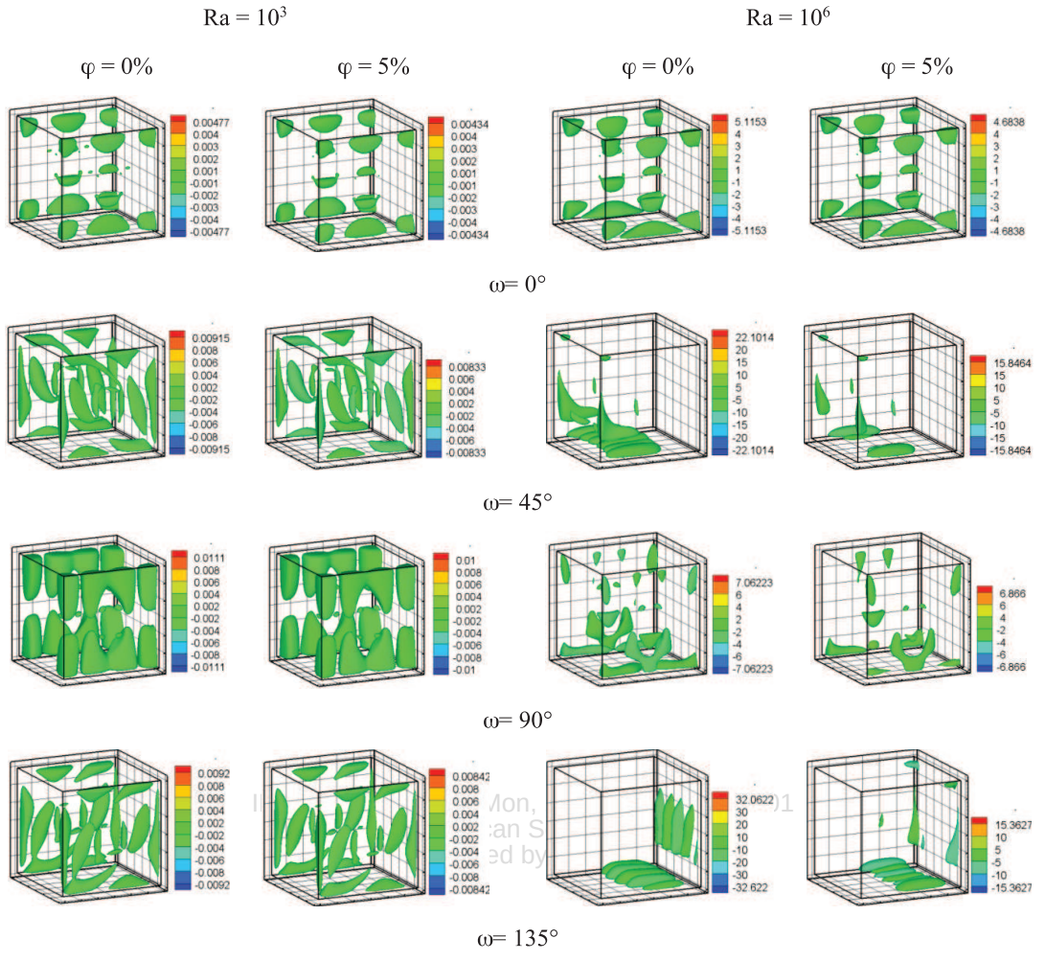

Fig. 14. Effect of inclination angles of magnetic field versus Rayleigh number and volume fraction of nanoparticles on *W*-velocity component isosurfaces.

imposed on the flow by the rear and front walls in the cubic configuration, compared with square configuration.

Figure 11 shows the isotherms structure in the presence of the magnetic field. When $Ra = 10^3$ and for all inclination angles of magnetic field, we can see that the isotherms structure of 2D configuration are similar to that of 3D configuration, and remain similar to those observed in the case $Ha = 0$. This is due to the predominance of conductive effects.

On the other hand, for $Ra = 10^6$, if we compare with the results carry out in the absence of the magnetic field, it appears that the isotherms become almost parallel to the vertical walls when the direction of the magnetic field is vertical. This is due to the large magnitude of the Lorentz force compared to the buoyancy force. Indeed, a strong heat gradient is observed in the upper left and right vertical walls, depending on whether the inclination of the angle is equal to 45° and 135°, respectively. In addition, the thermal boundary layer is thicker compared to the case without magnetic field, which results in a decrease in heat exchange. Regarding the effect of the presence of nanoparticles, there is a significant change at the bottom hot wall and the central area of the cavity, which means that the addition of nanoparticles enhances the heat exchange. Finally, if we compare the structure of the median plane isotherms ($Z = 0.50$) of the cubic cavity with that of the square cavity, we observe that for $\omega = 0°$ or $\omega = 90°$ the difference between 2D and 3D is less important. However, for the other angles, the difference is noticeable.

In the same way, as previously without magnetic field, we analyze and visualize three-dimensional distribution of the three velocity components (U, V and W) within the cubic cavity In the presence of the combined effects of the magnetic field, for different angles of inclination, and the variation of the buoyancy force, in the presence and the absence of nanoparticles. Indeed, the Figures 12–14 show that, the maximum values of the horizontal velocity (U) and the third velocity (W) are located far from the two median planes. So, graphically representing these two velocities in a central line is not representable. In addition, this figure shows also that the U-velocity is important and

ARTICLE

these values are significant compared to the V-velocity. Thus, it can be observed, the largest values of W-velocity are located near the six walls of the cubic cavity. Concerning the vertical velocity, the maximum value appears at the median plane and more precisely at the level of the two vortices. In the same figures, we note that increasing buoyancy force intensity causes a remarkable amplification of velocities magnitude, and the presence of 5% of nanoparticles in the base fluid causes a considerable decrease in the magnitude of the velocities. Finally, the Rayleigh number effect and the addition of nanoparticles depend on the Lorentz force direction.

In order to visualize the flow structure in the three-dimensional configuration, we present through Figure 15, the trajectories of some fluid particles, for two values of Rayleigh number ($Ra = 10^4$ and $Ra = 10^6$) and, in both cases, presence and absence of magnetic field, for two inclination angles 90° and 135°. In the case without magnetic field, this figure shows that the trajectories of the fluid particles are characterized by a three-dimensional behavior, and the circulation of the fluid particles is spiral-shaped in OZ direction. In addition, with increasing buoyancy force ($Ra = 10^6$), there is an intensification of recirculation zones. In the presence of the magnetic field ($Ha = 90$), it is observed that the recirculation zones are more ordered and less weak, when the direction of the magnetic field is vertical compared to the case $Ha = 0$. On the other hand, when $\omega = 135°$, fluid trajectories are narrower and vortex circulation becomes wider with respect to the case ($\omega = 90°$). Therefore, from this analysis, it can be concluded that the application of a vertical magnetic field causes a strong stability of the flow field.

5.3. Thermal Performance

Figure 16 shows, for various inclination angles of the magnetic field, the effect of Lorentz force intensity on heat exchange rate, within the two-dimensional cavity (square cavity) and the three-dimensional cavity (cubic cavity), for different Rayleigh numbers and with the presence and the absence of nanoparticles. The figure shows for both configurations (3D and 2D) that above $Ha = 30$, the variation of the Hartmann number has no influence on the heat exchange, in the case of the moderate Rayleigh number values ($Ra \leq 10^4$), given the low intensity of buoyancy forces. On the other hand, for high values of Rayleigh number and whatever the inclination angle of the magnetic field, increasing the intensity of Rayleigh number disadvantages the heat transfer. In addition, this figure shows for all parameters control considered, that the heat transfer rate is significantly high in the case of nanofluids compared to the base fluid. Indeed, the addition of alumina nanoparticles causes an increase in the fluid thermal conductivity,

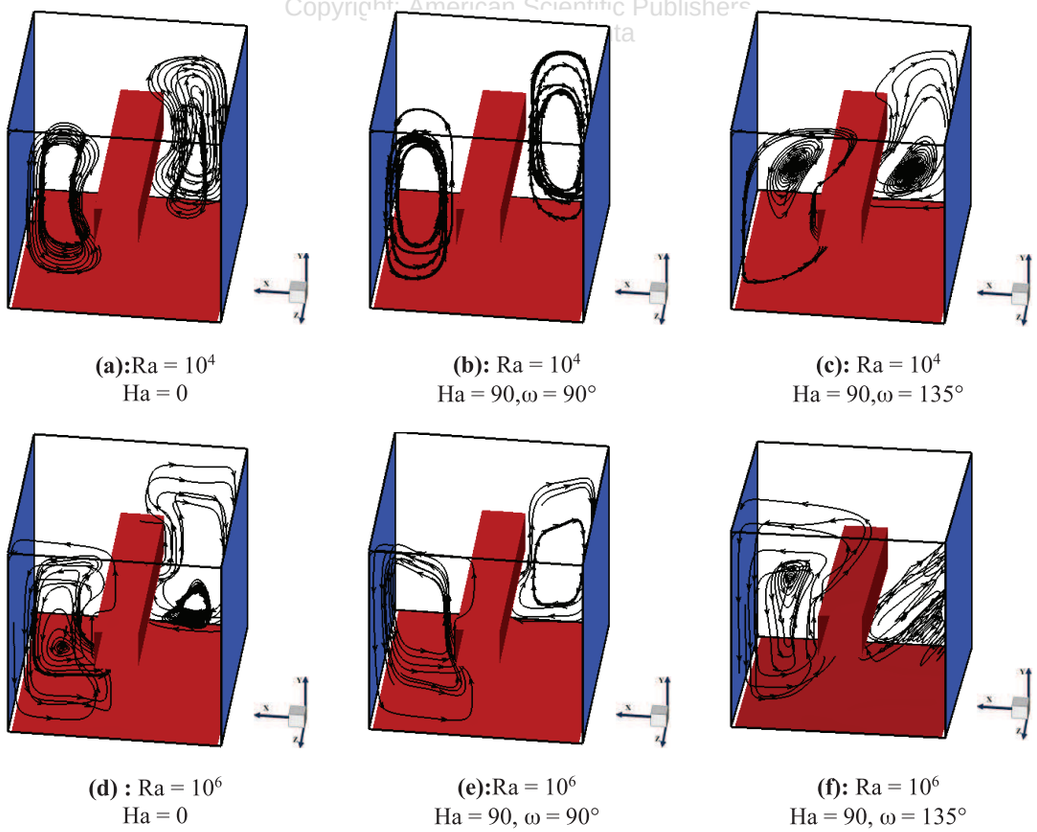

Fig. 15. Fluid particle pathlines for various pertinent parameters.

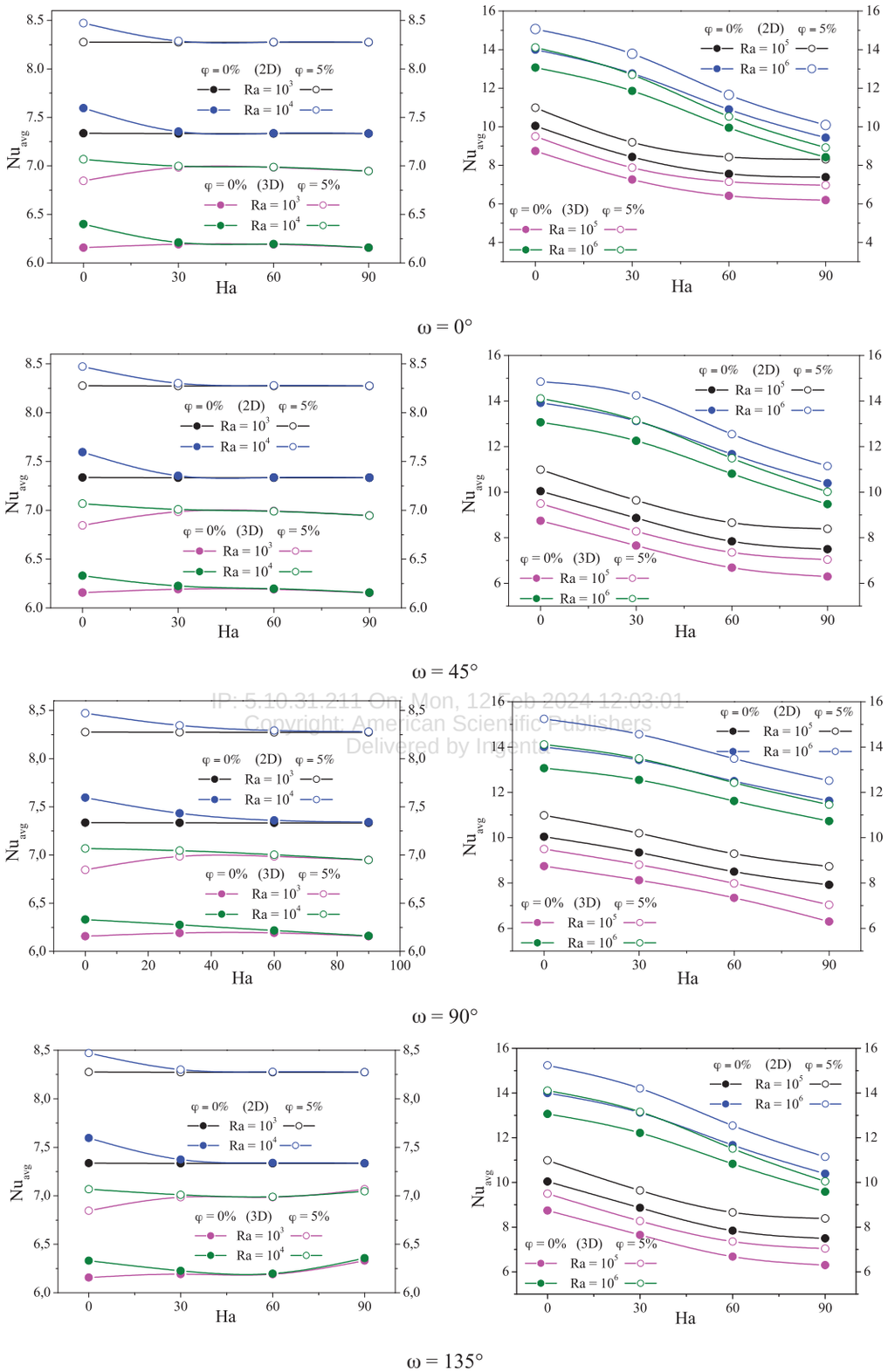

Fig. 16. Average Nusselt number for 2D and 3D configurations versus *Ra*, *Ha* and φ for different inclination angles of magnetic field.

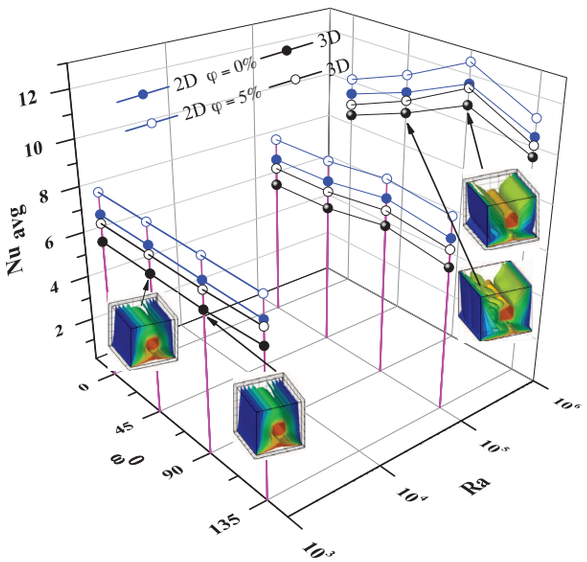

Fig. 17. Effects of inclination angle of magnetic field, Rayleigh number and nanoparticles volume fraction on the average Nusselt number for 2D and 3D configurations $Ha = 90$.

resulting in a higher heat transfer rate. Besides, we find that the average Nusselt number obtained by the square configuration is greater than that obtained by the cubic cavity, and this for all the control parameters considered.

Therefore, following these results, it can be concluded that taking into account the third direction is essential to have significant and representative results of a physical problem.

The 3D presentation of the average Nusselt number variation, depending on the control parameters, is shown through Figure 17. We observe that the parietal heat exchange rate is maximum when $\omega = 90°$, with an optimum (maximum) for the great Rayleigh number value ($Ra = 10^6$), for the case of presence and absence of nanoparticles. This is because the buoyancy and the magnetic forces act upwards, which corresponds to a situation of cooperative actions. For the case of a dominant thermal conduction ($Ra = 10^3$), the optimum is not visible.

5.4. Nanoparticles Performance

Figure 18, illustrates he Lorentz force effect on the evolution of the normalized average Nusselt number (Nu^*), calculated for different Rayleigh numbers and inclination angles of the magnetic field within the cavities (square and cubic). It appears that the addition of nanoparticles enhances the transfer rates, whatever of the values of Ra and ω. On the other hand, the best performances are observed for lower Rayleigh numbers ($Ra \leq 10^4$). Moreover, it should be noted that the inclination angle of the magnetic field has no effect on the improvement of the heat transfer rate, when $Ra = 10^3$. In addition, for $Ra = 10^4$, the best performance in the presence of the

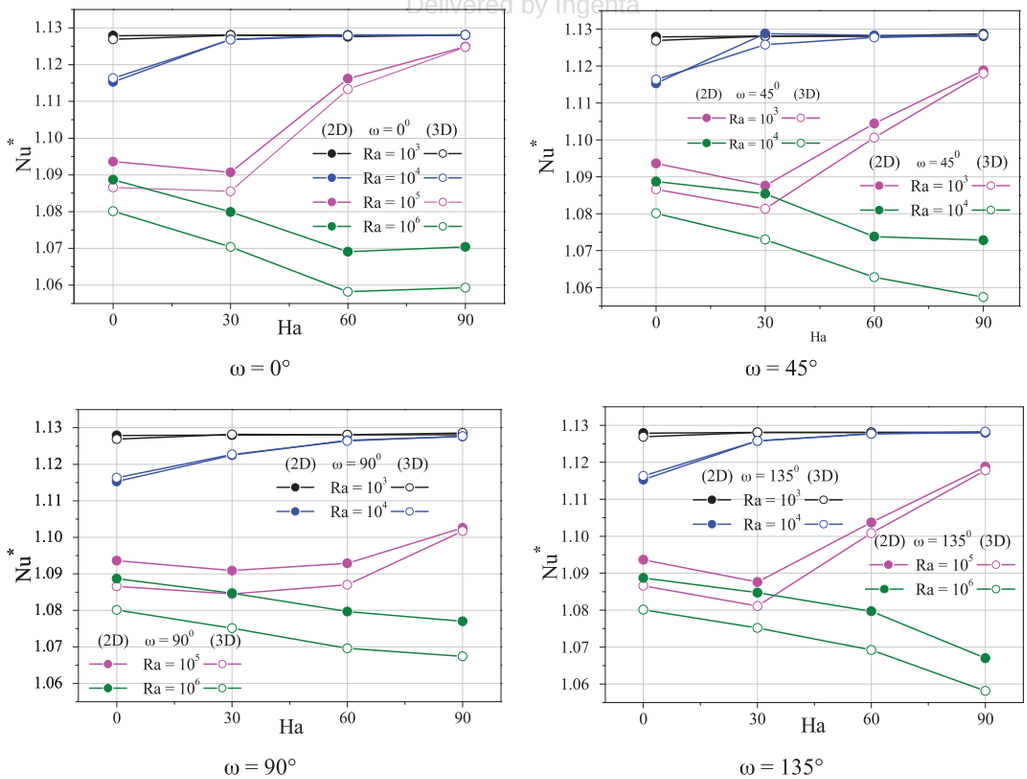

Fig. 18. Lorentz force effect on normalized Nusselt number for 2D and 3D configurations versus Rayleigh number for different inclination angles of the magnetic field.

magnetic field is obtained when $Ha \geq 60$ for all inclination angle of the magnetic field. Moreover, we observe that, for all inclination angles of the magnetic field, the gain reported on the heat exchange rate by the addition of nanoparticles is almost identical for low values of the Rayleigh number.

Whatever the value of the angle of inclination, a particular behavior is observed for $Ra = 10^5$, such as the normalized average Nusselt number decreases up to $Ha = 30$, after which it increases, reaching a maximum value at $Ha = 90$. For example, we found that increasing the Lorentz force magnitude from $Ha = 0$ to $Ha = 90$, increases the normalized average Nusselt number by 3.39%; 2.80%, 1.37%, and 2.79% for $\omega = 0°$, 45°, 90° and 135°; respectively. Finally, for $Ra = 10^6$, we note that when the Hartmann number increases, Nu* is greatly reduced for all inclination angles of magnetic field. This is due to the decrease of the kinetic energy, resulting from the increase in the Lorentz force.

The same previous figure shows also that the difference between 2D and 3D is negligible for the small values of Rayleigh number ($Ra \leq 10^4$) as well as the normalized Nusselt numbers obtained by the two-dimensional configuration is lower than those obtained by the three-dimensional configuration. On the other hand, a large difference between 2D and 3D is observed for high values of the Rayleigh number ($Ra \geq 10^5$) such as the values obtained for the 2D model are higher than those of the 3D model.

Based on the previous results, we plot the CM ratio (the merit coefficient of nanofluids) in terms of heat exchange rate, relative to 2D and 3D configurations, provided by the addition of nanoparticles, when the magnetic field is taken into account, compared to the case where the latter is absent.

The results are obtained for different Rayleigh numbers depending on the variation of inclination angle of the magnetic field, when $Ha = 90$ (Fig. 19). Thus, except the case $Ra = 10^6$, the addition of nanoparticles is beneficial ($CM \geq 1$) for 2D and 3D configurations, and the best performances are obtained for $\omega = 0°$.

Indeed, only the case $Ra = 10^6$ shows a disadvantage to the addition of nanoparticles ($CM < 1$), and that $\omega = 90°$ is the angle which relatively offers the best results. Note finally that the cases $Ra = 10^3$ and $Ra = 10^4$ show an independence of the results with respect to the angle ω.

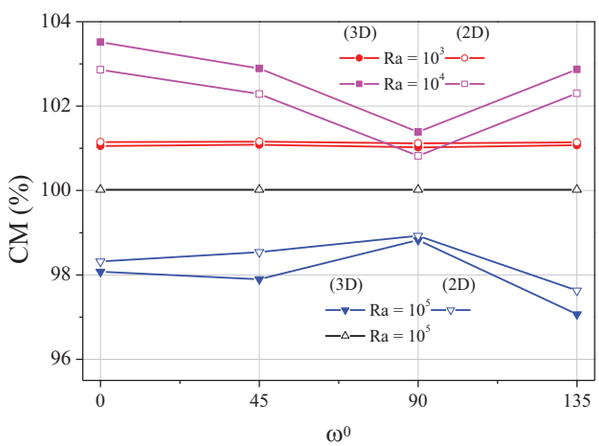

Fig. 19. Merit coefficient of nanoparticles for different inclination angles of the magnetic field and Rayleigh numbers for 2D and 3D configurations. $Ha = 90$.

6. CONCLUSION

In this work, the effects of three-dimensionality of the flow in existence of magnetic field and the addition of nanoparticles on heat exchange rate of natural convection in a cubic cavity were numerically studied. In addition, the effects of the main controlling parameters, such as Rayleigh number, inclination angles of magnetic field and Hartmann number were investigated. The following are the key conclusions that can be drawn from the findings.

(1) For higher *Ra* numbers, where the convection mechanisms controlled by the buoyancy force dominates, its heat transfer intensification becomes large, compared to the case where dominant conduction mechanism for lower *Ra* numbers.

(2) The addition of nanoparticles enhances heat transfer for both 2D and 3D configurations, and the best performance is obtained for $\omega = 0°$.

(3) The convective regime slows down when a magnetic field is added, and the amount of slowing relies on the Lorentz force applied, as well as the direction and intensity of the flow. Thus, the application of the magnetic field is related to the orientation of the Lorentz force, which can help or oppose the buoyancy force, or when the magnetic field is vertical ($\omega = 90°$), an optimal heat transfer rate occurs.

(4) In the presence of magnetic field, the addition of nanoparticles is beneficial for $Ra = 10^5$ and is less advantageous for $Ra = 10^3$ and 10^4. However, it is disadvantageous for $Ra = 10^6$.

(5) In the presence of the magnetic field ($Ha = 90$), it is observed that the recirculation zones are more ordered and less weak, when the direction of the magnetic field is vertical compared to the case $Ha = 0$.

(6) Increasing in the intensity of the buoyancy force causes a remarkable amplification in the flow structure, and the presence of 5% of nanoparticles in the base fluid causes a considerable decrease in velocities magnitude.

NOMENCLATURE

B_0	External magnetic field (T)
C_p	Constant pressure specific heat (J kg^{-1} K^{-1})
F	Lorentz force (N m^{-3})
g	Gravitational acceleration (m s^{-2})
J	The electric current density (A/m^2)

H Height of cavity (m)
Ha Hartman number, $B_0 L\sqrt{\sigma_f/\rho_f \nu_f}$
k Thermal conductivity ($W\,m^{-1}\,K^{-1}$)
L Length of the cavity (m)
Nu Nusselt number, $Nu = \left(-\frac{k_{nf}}{k_{bf}}\right)\frac{\partial\theta}{\partial X}\Big|_{wall}$
p Pressure (Pa)
P Dimensionless pressure, $pH/\rho_f\alpha_f^2$
Pr Prandtl number, ν_f/α_f
Re Reynolds number, $V_0 H/\nu_f$
T Temperature (K)
u, v, w Velocity components in the x-direction, y-direction and z-direction ($m\,s^{-1}$)
U, V, W Dimensionless velocity components
x, y, z Cartesian coordinates (m)
X, Y, Z Dimensionless Cartesian coordinates

Greek Symbols

α Thermal diffusivity ($m^2\,s^{-1}$)
β Thermal expansion coefficient (K^{-1})
θ Dimensionless temperature
μ Dynamic viscosity ($kg\,m^{-1}\,s^{-1}$)
ν Kinematic viscosity ($m^2\,s^{-1}$)
ρ Density ($kg\,m^{-3}$)
σ Electrical conductivity ($\Omega^{-1}\,m^{-1}$)
φ Particle volume fraction
ω Inclination angles of the magnetic field

Superscript

Avg Average
bf Base fluid
nf Nanofluid
s Solid particles
0 References
2D Two-dimensional
3D Three-dimensional

Conflicts of Interest

The authors declare no conflicts of interest.

Acknowledgments: This work was supported by the Ministry of Higher Education and Scientific Research of Algeria with granted contracts (No. A11N01UN440120220001).

References and Notes

1. A. E. Kabeel, E. M. El-Said, and S. A. Dafea, *Renewable and Sustainable Energy Reviews* 45, 830 (**2015**).
2. A. S. Dogonchi, K. Divsalar, and D. D. Ganji, *Computer Methods in Applied Mechanics and Engineering* 310, 58 (**2016**).
3. M. Benzema, Y. K. Benkahla, N. Labsi, E. Brunier, and S. E. Ouyahia, *Arabian Journal for Science and Engineering* 42, 4575 (**2017**).
4. N. S. Bondareva and M. A. Sheremet, *Int. J. Heat Mass Transfer* 108, 1057 (**2017**).
5. S. A. Zonouzi, H. Aminfar, and M. Mohammadpourfard, *Appl. Therm. Eng.* 151, 11 (**2019**).
6. S. U. Choi and J. A. Eastman, Enhancing Thermal Conductivity of Fluids with Nanoparticles (No. ANL/MSD/CP-84938; CONF-951135-29), Argonne National Lab. (ANL), Argonne, IL (United States) (**1995**).
7. M. J. Assael, K. D. Antoniadis, W. A. Wakeham, and X. Zhang, *Int. J. Heat Mass Transfer* 138, 597 (**2019**).
8. R. Saidur, K. Y. Leong, and H. A. Mohammed, *Renewable and Sustainable Energy Reviews* 15, 1646 (**2011**).
9. F. S. Javadi, R. Saidur, and M. Kamalisarvestani, *Renewable and Sustainable Energy Reviews* 28, 232 (**2013**).
10. S. M. Vanaki, P. Ganesan, and H. A. Mohammed, *Renewable and Sustainable Energy Reviews* 54, 1212 (**2016**).
11. K. S. Suganthi and K. S. Rajan, *Renewable and Sustainable Energy Reviews* 76, 226 (**2017**).
12. M. Hemmat Esfe, M. Akbari, and A. Karimipour, *Journal of Applied Mechanics and Technical Physics* 56, 443 (**2015**).
13. A. M. Rashad, S. E. Ahmed, M. A. Mansour, T. Salah, and H. A. Nabwey, *Journal of Porous Media* 23, 805 (**2020**).
14. K. Ragui, Y. Benkahla, N. Labsi, and A. Boutra, Natural Heat Transfer Convection in a Square Cavity Including a Square Heater, *21th Congrès Français de Mécanique, Bordeaux* (**2013**), Vol. 26.
15. A. R. Rahmati and A. A. Tahery, *Alexandria Engineering Journal* 57, 1271 (**2018**).
16. F. Garoosi and M. M. Rashidi, *International Journal of Mechanical Sciences* 131, 1026 (**2017**).
17. S. Izadi, T. Armaghani, R. Ghasemiasl, A. J. Chamkha, and M. Molana, *Powder Technol.* 343, 880 (**2019**).
18. M. A. Mansour, S. E. Ahmed, and A. M. Rashad, *Journal of Applied Fluid Mechanics* 9, 2515 (**2016**).
19. S. E. Ahmed, A. M. Rashad, and R. S. Reddy Gorla, *J. Thermophys Heat Transfer* 27, 700 (**2013**).
20. T. Armaghani, A. Chamkha, A. M. Rashad, and M. A. Mansour, *J. Therm. Anal. Calorim.* 142, 2273 (**2020**).
21. B. Ghasemi, S. M. Aminossadati, and A. Raisi, *International Journal of Thermal Sciences* 50, 1748 (**2011**).
22. M. M. Rahman, S. Mojumder, S. Saha, A. H. Joarder, R. Saidur, and A. G. Naim, *Int. J. Heat Mass Transfer* 89, 1316 (**2015**).
23. G. R. Kefayati, *Int. J. Heat Mass Transfer* 92, 1066 (**2016**).
24. M. S. Sadeghi, N. Anadalibkhah, R. Ghasemiasl, T. Armaghani, A. S. Dogonchi, A. J. Chamkha, H. Ali, and A. Asadi, *J. Therm. Anal. Calorim.* 43, 1 (**2020**).
25. F. Selimefendigil and H. F. Öztop, *Journal of the Taiwan Institute of Chemical Engineers* 56, 42 (**2015**).
26. A. M. Rashad, A. J. Chamkha, M. A. Ismael, and T. Salah, *J. Heat Transfer* 140, 072501 (**2018**).
27. T. Javed and M. A. Siddiqui, *International Journal of Thermal Sciences* 125, 419 (**2018**).
28. K. A. Ayoubloo, M. Ghalambaz, T. Armaghani, A. Noghrehabadi, and A. J. Chamkha, *International Journal of Numerical Methods for Heat and Fluid Flow* 30, 1096 (**2019**).
29. T. Armaghani, A. Chamkha, A. M. Rashad, and M. A. Mansour, *J. Therm. Anal. Calorim.* 142, 2273 (**2020**).
30. S. Hussain, K. Mehmood, and M. Sagheer, *J. Magn. Magn. Mater.* 419, 140 (**2016**).
31. Q. Xiong, E. Abohamzeh, J. A. Ali, S. M. Hamad, I. Tlili, A. Shafee, H. Habibeh, and T. K. Nguyen, *J. Mol. Liq.* 292, 111386 (**2019**).
32. A. I. Alsabery, T. Armaghani, A. J. Chamkha, M. A. Sadiq, and I. Hashim, *International Journal of Numerical Methods for Heat and Fluid Flow* 29, 1272 (**2018**).
33. M. Benzema, Y. K. Benkahla, N. Labsi, S. E. Ouyahia, and M. El Ganaoui, *J. Therm. Anal. Calorim.* 137, 1113 (**2019**).
34. P. X. Yu and Z. F. Tian, *Applied Mathematical Modelling* 41, 143 (**2017**).
35. H. Ozoe and K. Okada, *Int. J. Heat Mass Transfer* 32, 1939 (**1989**).

36. G. R. Kefayati and H. Tang, *Int. J. Heat Mass Transfer* 124, 344 **(2018)**.
37. A. A. Al-Rashed, L. Kolsi, H. F. Oztop, A. Aydi, E. H. Malekshah, N. Abu-Hamdeh, and M. N. Borjini, *Physica E: Low-Dimensional Systems and Nanostructures* 99, 294 **(2018)**.
38. A. M. Rashad, T. Armaghani, A. J. Chamkha, and M. A. Mansour, *Chinese Journal of Physics* 56, 193 **(2018)**.
39. M. A. Mansour, R. S. R. Gorla, S. Siddiqa, A. M. Rashad, and T. Salah, *International Journal of Nonlinear Sciences and Numerical Simulation* 000010151520200138 **(2021)**, DOI: 10.1515/ijnsns-2020-0138.
40. S. Hussain, T. Armaghani, and M. Jamal, *J. Thermophys. Heat Transfer* 34, 203 **(2020)**.
41. A. Purusothaman, H. F. Oztop, N. Nithyadevi, and N. H. Abu-Hamdeh, *Computers and Fluids* 128, 30 **(2016)**.
42. M. Sheikholeslami, S. A. Shehzad, and Z. Li, *Int. J. Heat Mass Transfer* 125, 375 **(2018)**.
43. A. M. Rashad, R. S. R. Gorla, M. A. Mansour, and S. E. Ahmed, *Journal of Porous Media* 20, 363 **(2017)**.
44. I. Jelodari and A. H. Nikseresht, *J. Mol. Liq.* 252, 296 **(2018)**.
45. J. K. Zhang, B. W. Li, H. Dong, X. H. Luo, and H. Lin, *Int. J. Heat Mass Transfer* 112, 216 **(2017)**.
46. S. Kherroubi, K. Ragui, A. Bensaci, N. Labsi, A. Boutra, and Y. K. Benkahla, *J. Therm. Anal. Calorim.* 139, 2243 **(2020)**.
47. F. Selimefendigil and H. F. Öztop, *Int. J. Heat Mass Transfer* 137, 650 **(2019)**.
48. G. R. Kefayati and H. Tang, *Int. J. Heat Mass Transfer* 131, 346 **(2019)**.
49. M. Sheikholeslami and H. B. Rokni, *Int. J. Heat Mass Transfer* 115, 1203 **(2017)**.
50. E. Sourtiji, M. Gorji-Bandpy, D. D. Ganji, and S. F. Hosseinizadeh, *Powder Technol.* 262, 71 **(2014)**.
51. M. Corcione, *Energy Convers. Manage.* 52, 789 **(2011)**.
52. M. Cianfrini, M. Corcione, and A. Quintino, *Thermal Science* 19, 591 **(2015)**.
53. M. Corcione, M. Cianfrini, and A. Quintino, *Int. J. Heat Mass Transfer* 88, 902 **(2015)**.
54. S. Kherroubi, Y. K. Benkahla, A. Boutra, and A. Bensaci, *J. Therm. Anal. Calorim.* 147, 1859 **(2022)**.
55. K. M. Khanafer and A. J. Chamkha, *Int. J. Heat Mass Transfer* 42, 2465 **(1999)**.
56. S. V. Patankar, *Numerical Heat Transfer and Fluid Flow*, Hemisphere Publ. Corp., New York **(1980)**, Vol. 58, p. 288.
57. P. X. Yu, J. X. Qiu, Q. Qin, and Z. F. Tian, *Int. J. Heat Mass Transfer* 67, 1131 **(2013)**.
58. R. J. Krane, Some Detailed Field Measurements for a Natural Convection Flow in a Vertical Square Enclosure, *Proceedings of the First ASME-JSME Thermal Engineering Joint Conference, 1983* **(1983)** Vol. 1, pp. 323–329.
59. K. Khanafer, K. Vafai, and M. Lightstone, *Int. J. Heat Mass Transfer* 46, 3639 **(2003)**.
60. P. Ternik, *Int. J. Heat Mass Transfer* 80, 368 **(2015)**.